International Journal of Bifurcation and Chaos, Vol. 1, No. 1 (1991) 27–50

THE GEOMETRY AND COMPUTATION OF THE DYNAMICS OF COUPLED PENDULA

M. E. HENDERSON
Dept. of Mathematical Sciences, IBM Research, T. J. Watson Res. Center, P.O. Box 218, Yorktown Heights, NY, USA

M. LEVI
Dept. of Mathematics, Boston University, Boston, MA 02215, USA

F. ODEH
Dept. of Mathematical Sciences, IBM Research, T. J. Watson Res. Center, P.O. Box 218, Yorktown Heights, NY, USA

Received June 3, 1990; Revised July 19, 1990

In this paper, we analyze the dynamics of a system consisting of two torsionally coupled pendula with dissipation and with external forcing. In addition to several general results about the periodic solutions of the system, we prove that a family of homoclinic solutions exists in part of the parameter space, and give computational evidence that part of this family is the type considered by Shil'nikov. The existence of such orbits generates rich dynamics, which we describe qualitatively and illustrate with computed solutions.

1. Introduction

In this paper, we analyze the dynamics of a system consisting of two torsionally coupled pendula with dissipation and with external forcing:

$$\ddot{\phi}_1 + \gamma\dot{\phi}_1 + \sin\phi_1 + k(\phi_1 - \phi_2) = I_1 ,$$

$$\ddot{\phi}_2 + \gamma\dot{\phi}_2 + \sin\phi_2 + k(\phi_2 - \phi_1) = I_2 . \quad (1.1)$$

Besides being of intrinsic interest as a natural extension of the classical model of a single pendulum, this system describes several physical phenomena such as SQUIDs (Superconducting Quantum Interference Devices) and charge-density waves.

Some major advances in the *geometric* theory of dynamical systems have been slow in being applied to differential equations because, although "it is useful to solve differential equations" (Arnold's paraphrasing of Euler [Arnold, 1983]), it is difficult to do so, i.e., to extract the geometrical information from the analytic expressions. Thus very few physical systems with 2 degrees of freedom have been understood geometrically. The notable exceptions are the cases when extra structure is present, e.g., complete integrability or a small parameter.

In this paper, we combine the results of numerical and geometric approaches to predict, describe and explain some observable features of the system. One such feature is a very transparent physical manifestation of the Shil'nikov bifurcation [Ovsyannikov & Shil'nikov, 1987] — one can observe the geometrical phenomenon in $\mathbf{R}^4$ by simply watching the coupled pendula tumble.

1.1. *A single pendulum*

A single shunted Josephson junction [Feynman, 1963] is described by the well-known and well-understood equation of the single driven, damped pendulum:

$$\ddot{\phi} + \lambda\dot{\phi} + \sin\phi = I ; \quad (1.2)$$

this equation is one of the basic simple models in the theory of dynamical systems. It also arises in various other applications such as charge-density waves [Grüner & Zettl, 1985] and electromechanical problems of dynamos [Tricomi, 1931; Amerio, 1949]. Mathematically, this system has been well understood for many decades [Amerio, 1949; Tricomi, 1931; Andronov *et al.*, 1949]. The dynamic behavior becomes much more complicated if I is allowed to vary in time. It is well known that if the forcing depends periodically on time ($I = I(t)$) the problem is beyond the possibility of complete analysis. In fact, the simple example of the periodically forced pendulum exhibits virtually all the behavior that has been understood so far in low-dimensional geometrical theory of dynamical systems: KAM theory [Moser, 1973], Aubry–Mather theory [Aubry & LeDaeron, 1983; Mather, 1982], hyperbolic theory (horseshoes) [Moser, 1973], bifurcation theory [Arnold, 1983], Benedicks–Carleson theory [Benedicks & Carleson, 1988], etc., with some questions still unanswered.

1.2. *Coupled pendula*

The case of two or more coupled pendula offers even less hope for a complete understanding, and we readjust our goals. In certain parameter ranges, one can still obtain a good understanding of the behavior; for instance, in the case of two coupled pendula (1.1) the regime of large coupling coefficient k has been studied in several papers [Imry & Schulman, 1978; Zimmerman & Sullivan, 1977]; the system behaves as a single damped pendulum (for fixed $\gamma > 0$ and sufficiently large k). In the opposite extreme, that of small k, the dynamics is richer but the system has been understood virtually completely in this range as well. In this paper, we combine geometrical and numerical analyses to study the dynamics of Eq. (1.1) in the range of moderate coupling k.

To give some intuition which will be relevant in our later discussion of other parameter ranges, we describe the behavior of Eq. (1.1) for the case of small coupling k. We provide a heuristic discussion of the 'caterpillar' solutions; the details and the proofs can be found in Levi [1988]. To simplify the discussion, we take $I_2 = 0$. Assume that one pendulum, say ϕ_1, starts near a slowly moving sink of the first equation

$$\ddot{\phi}_1 + \gamma\dot{\phi}_1 + \sin\phi_1 + k\phi_1 = k\phi_2 + I_1 \ , \quad (1.3a)$$

with the right-hand side treated as a near-constant — we are looking at the case of small k. Assume that the other pendulum, ϕ_2, is meanwhile running according to its equation

$$\ddot{\phi}_2 + \gamma\dot{\phi}_2 + \sin\phi_2 + k\phi_2 = k\phi_1 \ , \quad (1.3b)$$

Now, *if* a caterpillar solution is to exist, then ϕ_1 will have to start, i.e., the sink in Eq. (1.3a) which has held ϕ_1 must disappear in a saddle-node bifurcation at about the same time that ϕ_2 stops running, i.e., when Eq. (1.3b) with the right-hand side treated as a constant acquires a heteroclinic connection. Thus, heuristically, a necessary condition for a caterpillar solution to exist is the near-simultaneous occurrence of the saddle-node bifurcation for one pendulum with the heteroclinic bifurcation for the other.

There have been several numerical studies of the coupled pendula using numerical integration schemes to compute the stable periodic motions, for example Marcus & Imry [1980] and Imry & Schulman [1978]. More recently, Aronson, Doedel and Othmer [1991] have investigated the bifurcation of periodic solutions as a function of the coupling strength k for small damping and $I_1 = I_2$. In Doedel *et al.* [1988] periodic solutions were computed using a two-point, boundary-value problem, and unstable periodic motions and bifurcation diagrams were presented. In Aronson *et al.* [1991] the limit of zero damping was considered, also on $I_1 = I_2$. In this limit, the equations become Hamiltonian and a family of periodic solutions exists. It is shown in Aronson *et al.* [1991] that, as the damping is increased from zero, bifurcations from the Hamiltonian family give rise to a large number of periodic motions, which disappear in turn as the damping becomes larger.

In this paper we consider the damping γ and the coupling strength k to be fixed, and investigate the (I_1, I_2)-plane. This is physically realistic, since the torques can be changed without modifying the apparatus, and is consistent with the calculations of Marcus & Imry [1980]. We consider the evolution of one class of solutions from the line $I_1 = I_2$ (those connected to the synchronous solution) as the difference between the torques is changed. We do not find, for example, the periodic solutions with "winding number" three (these exist for smaller coupling strengths on $I_1 = I_2$, and may still be present in the range of k discussed here).

1.3. *Results: An outline*

We begin by stating some of the basic properties of Eq. (1.1) and its solutions. These include the Hamiltonian form of (1.1); its symmetries, which

reduce the parameter space to a fundamental wedge and generate surfaces in the parameter space along which "symmetric" solutions exist; and finally a discussion of the equilibrium points of Eq. (1.1), their stability and bifurcation behavior.

In Sec. 2 we describe how the periodic solution branches presented here were computed, and show that when the damping γ is nonzero, the Floquet multipliers of a periodic motion may cross the unit circle only at ± 1. This eliminates the possibility of bifurcation to higher period than period doubling (e.g., period tripling), bifurcation to quasiperiodic solutions and torus bifurcation.

Section 3 describes the behavior of periodic solutions near a "Shil'nikov bifurcation" in terms of a Poincaré map. In Sec. 4, we present the main theoretical result of this paper: that a family of homoclinic connections exists for moderately large coupling strengths k. This family may be parametrized by the difference of the two applied torques $I_1 - I_2$, and crosses the entire fundamental wedge in parameter space. The coupling strength must be sufficiently large that only one pair of equilibrium points exists. In Sec. 5, we present the results of computations of this family of homoclinic connections at a smaller coupling strength, at which a moderate number of equilibrium points exist. These results indicate that the family of homoclinic solutions still exists, and that it interacts with the additional equilibrium points.

In Sec. 6, we interpret the motion of the pendula in terms of the periodic motions near the Shil'nikov bifurcation. We show, for instance, that for any given integer N there is an open set in parameter space in which a *stable* periodic solution exists whose behavior can be loosely described as near-simultaneous tumbles of the pendula with N relative oscillations per tumble. We also point out that heteroclinic Shil'nikov bifurcation may also occur in this problem.

Finally, in Sec. 7, we make some comments about the relationship of these computed solutions to the "caterpillar" solutions, whose existence has been proved for much smaller coupling strengths.

2. Qualitative and Numerical Analysis

2.1. *General facts*

We begin by presenting some easily derived facts about the coupled pendula.

2.1.1. *The Hamiltonian character of the equations*

Equation (1.1) is equivalent to the damped Hamiltonian system

$$\dot{x} = J\nabla_x H - \gamma D x \,, \tag{2.1}$$

where

$$J = \begin{pmatrix} 0 & I \\ -I & 0 \end{pmatrix}, \quad D = \begin{pmatrix} 0 & 0 \\ 0 & I \end{pmatrix},$$
$$x = \mathrm{col}(\phi_1, \phi_2, \dot{\phi}_1, \dot{\phi}_2), \quad I = \begin{pmatrix} 1 & 0 \\ 0 & 1 \end{pmatrix},$$

with Hamiltonian

$$H(\phi_1, \phi_2, \dot{\phi}_1, \dot{\phi}_2) = \frac{1}{2}((\dot{\phi}_1)^2 + (\dot{\phi}_2)^2) - (\cos\phi_1 + \cos\phi_2) + \frac{1}{2}k(\phi_1 - \phi_2)^2 - I_1\phi_1 - I_2\phi_2 \,.$$

Differentiation of H along the flow gives

$$\frac{dH}{dt} = \nabla_x H\dot{x} = -\gamma((\dot{\phi}_1)^2 + (\dot{\phi}_2)^2) \le 0 \,, \tag{2.2}$$

so along a trajectory the energy H is decreasing.

An alternative formulation of (1.1) which is sometimes convenient is in terms of the half-angle between the pendula, ξ, and the mean position of the pendula, η

$$\xi = \frac{1}{2}(\phi_1 - \phi_2)$$

$$\eta = \frac{1}{2}(\phi_1 - \phi_2) \,;$$

Eqs. (1.1) become

$$\begin{aligned} \ddot{\xi} + \gamma\dot{\xi} + \sin\xi\cos\eta + 2k\xi &= I_c \\ \ddot{\eta} + \gamma\dot{\eta} + \sin\eta\cos\xi &= I \,, \end{aligned} \tag{2.3}$$

where

$$I_c = \frac{1}{2}(I_1 - I_2)$$

$$I = \frac{1}{2}(I_1 + I_2) \,.$$

In these variables, the system is 2π periodic in η, and

the Hamiltonian is

$$H(\xi, \eta, \dot{\xi}, \dot{\eta}) = \frac{1}{2}(\dot{\xi})^2 + \frac{1}{2}(\dot{\eta})^2 - \cos\xi\cos\eta + k\xi^2 - I_c\xi - I\eta \ .$$

2.1.2. *The symmetries of Eq. (1.1)*

Equation (1.1) has several symmetries. Together, these reduce the four-dimensional parameter space $\{(I_1, I_2, k, \gamma) \mid k, \gamma \geq 0)\}$ to a fundamental wedge whose intersection with the plane $\{k = \text{const}, \gamma = \text{const}\}$ is a strip of width $k\pi$ in the $I_1 I_2$ plane. Equation (1.1) is invariant under the following operations:
a) Permutation of the indices:

$$(\phi_1, \phi_2, \dot{\phi}_1, \dot{\phi}_2, I_1, I_2, k, \gamma) \to (\phi_2, \phi_1, \dot{\phi}_2, \dot{\phi}_1, I_2, I_1, k, \gamma)$$

b) Reflection of $\{\phi_1, \phi_2\}$ and $\{I_1, I_2\}$:

$$(\phi_1, \phi_2, \dot{\phi}_1, \dot{\phi}_2, I_1, I_2, k, \gamma) \to$$

$$(-\phi_1, -\phi_2, -\dot{\phi}_1, -\dot{\phi}_2, -I_1, -I_2, k, \gamma)$$

c) 2π translation of η:

$$(\phi_1, \phi_2, \dot{\phi}_1, \dot{\phi}_2, I_1, I_2, k, \gamma) \to$$

$$(\phi_1 + 2\pi, \phi_2 + 2\pi, \dot{\phi}_1, \dot{\phi}_2, I_1, I_2, k, \gamma)$$

d) $2k\pi$ translation of I_c:

$$(\phi_1, \phi_2, \dot{\phi}_1, \dot{\phi}_2, I_1, I_2, k, \gamma) \to$$

$$(\phi_1 + 2\pi, \phi_2, \dot{\phi}_1, \dot{\phi}_2, I_1 + 2k\pi, I_2 - 2k\pi, k, \gamma)$$

Together these reduce the parameter space to the fundamental wedge

$$I = \frac{(I_1 + I_2)}{2} \in [0, \infty) \quad I_c = \frac{(I_1 + I_2)}{2} \in [0, k\pi)$$

$$k \in [0, \infty) \quad \gamma \in [0, \infty) \ .$$

Along the edges of this domain, symmetric solutions may exist. On $I_c = k\pi$ symmetric running solutions of period T (see Sec. 2.3) satisfy

$$\xi(t + T/2) = \pi - \xi(t),$$
$$\eta(t + T/2) = \eta(t) + \pi \ . \qquad (2.4)$$

On $I = 0$, symmetric solutions satisfy

$$\ddot{\xi} + \gamma\dot{\xi} + \sin\xi + 2k\xi = I_c,$$
$$\eta = 0 \ . \qquad (2.5)$$

That is, for $I = 0$, the two-dimensional phase plane $\{\phi_1 = -\phi_2, \dot{\phi}_1 = -\dot{\phi}_2\}$ is an invariant submanifold of the full phase space $\mathbb{R}^4$. On this submanifold, the motion is equivalent to a single pendulum with a linear restoring force, which is discussed in Levi [1988] in connection with the caterpillar solutions in double pendula equations.

On $I_c = 0$, the symmetric solutions are determined by:

$$\xi = 0,$$
$$\ddot{\eta} + \gamma\dot{\eta} + \sin\eta = I \ . \qquad (2.6)$$

That is, for $I_c = 0$, the subspace $\{\phi_1 = \phi_2, \dot{\phi}_1 = \dot{\phi}_2\}$ is an invariant submanifold of the full phase space. The dynamics on this submanifold corresponds to the motion of a single damped pendulum. Figure 1 summarizes its behavior.

For $I < 1$, there are two equilibrium points on the invariant submanifold, one a stable center, the other a saddle. For $I > 1$, there are no equilibrium points, and

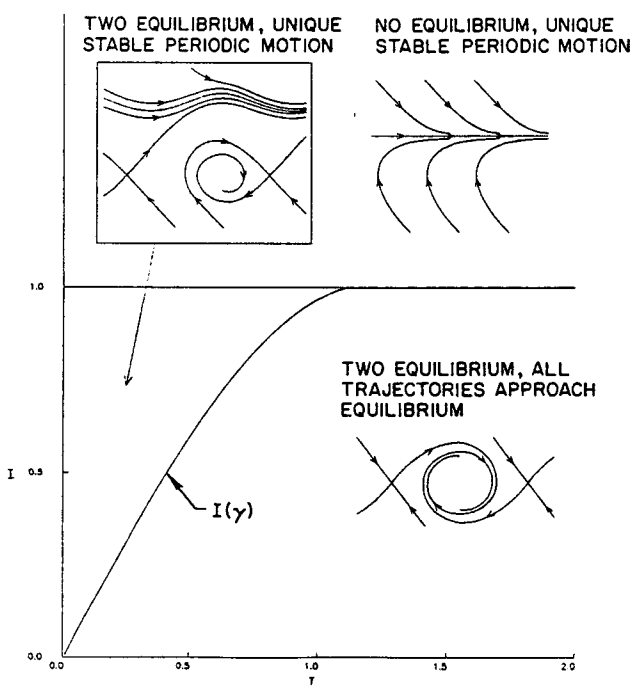

Fig. 1. The dynamics of the single, damped pendulum.

a curve $I(\gamma)$ exists such that $I < I(\gamma)$ there are no periodic solutions on the submanifold. For $I > I(\gamma)$, there is a unique stable periodic solution. On $I = I(\gamma)$, a homoclinic connection exists from the saddle to its periodic repetition.

In each case, nonsymmetric solutions of (1.1) may coexist with these symmetric solutions, and may be connected to a branch of symmetric solutions via symmetry-breaking bifurcations.

2.2. *Equilibrium points*

The principal focus of this paper is on the homoclinic solutions of (1.3) and the periodic solutions associated with them. The structure of the branches of periodic solutions depends on the stability of the hyperbolic equilibrium point associated with the homoclinic solution. Hence, we begin our analysis with a brief description of the equilibrium points of (1.1) and their stability. By parametrizing the equilibrium points by the half-angle ξ between the two pendula, it is possible to compute explicitly all the equilibrium points. We have used this technique to produce the figures below.

2.2.1. *Existence of equilibrium points*

The equilibrium points of (1.1) are determined by

$$\begin{aligned} \sin\xi\cos\eta + 2k\xi &= I_c \\ \sin\eta\cos\xi &= I \,. \end{aligned} \tag{2.7}$$

Therefore, equilibrium points exist only for

$$\frac{I_c - 1}{2k} \le \xi \le \frac{I_c + 1}{2k}, \quad I \le |\cos\xi|, \quad \text{and} \quad I \le |\sin\eta| \,. \tag{2.8}$$

For $|I| > 1$, no equilibrium points exist. Figure 2 shows the equilibrium points as a function of I for $k = 0.1$ and $I_c = k\pi/2$. Figure 3 shows the half-angle ξ at the equilibrium point as a function of both I_1 and I_2 for the several values of k.

The different "figure 8" curves in each π interval of ξ correspond to a "winding up" of the pendula. For weak coupling, increasing the separation of the pendula by 2π alters the applied torques by a small amount ($I_c \to I_c + 2k\pi$). This explains the large number of equilibria for small k. (For larger values of k, most of these equilibria disappear in a sequence of saddle-node bifurcations.)

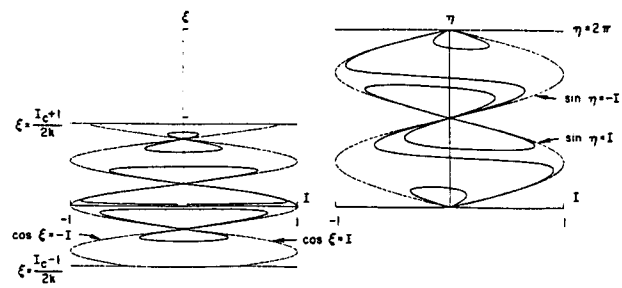

Fig. 2 The equilibrium points of the coupled pendula as a function of the applied torque I for $k = 0.1$, $I_c = k\pi/2$.

2.2.2. *Stability of equilibrium points*

To determine the stability of an equilibrium solution ($\Phi = (\phi_1, \phi_2, 0, 0)$) of (1.1), we linearize the system in its Hamiltonian form (2.1), obtaining for the perturbation $\mathbf{X}, \dot{\mathbf{X}} = (JH''(\Phi) - \gamma D)\mathbf{X} \equiv A\mathbf{X}$, where

$$A = \begin{pmatrix} 0 & 0 & 1 & 0 \\ 0 & 0 & 0 & 1 \\ -a & k & -\gamma & 0 \\ k & -b & 0 & -\gamma \end{pmatrix}, \quad \text{with} \quad \begin{aligned} a &= \cos\phi_1 + k \\ b &= \cos\phi_2 + k \end{aligned} .$$

We find that A has eigenvalues $\lambda_{nm} = -\gamma/2 + (-1)^n \sqrt{\frac{1}{4}\gamma^2 + \alpha_m}$, $(m, n = 0, 1)$ and the corresponding left and right eigenvectors

$$w_{nm} = \begin{pmatrix} (\lambda_{nm} + \gamma)k \\ (\lambda_{nm} + \gamma)(a + \alpha_m) \\ k \\ a + \alpha_m \end{pmatrix},$$

$$v_{nm} = \begin{pmatrix} k \\ a + \alpha_m \\ \lambda_{nm}k \\ \lambda_{nm}(a + \alpha_m) \end{pmatrix},$$

where

$$\alpha_m = -(a + b)/2 + (-1)^m \sqrt{(a - b)^2/4 + k^2} \,.$$

Since the real part of any complex eigenvalue must be $-\gamma/2$, there can be no Hopf bifurcation. It is also not possible for two eigenvalues to be zero at the same time, so all bifurcations of equilibrium points must be simple bifurcations.

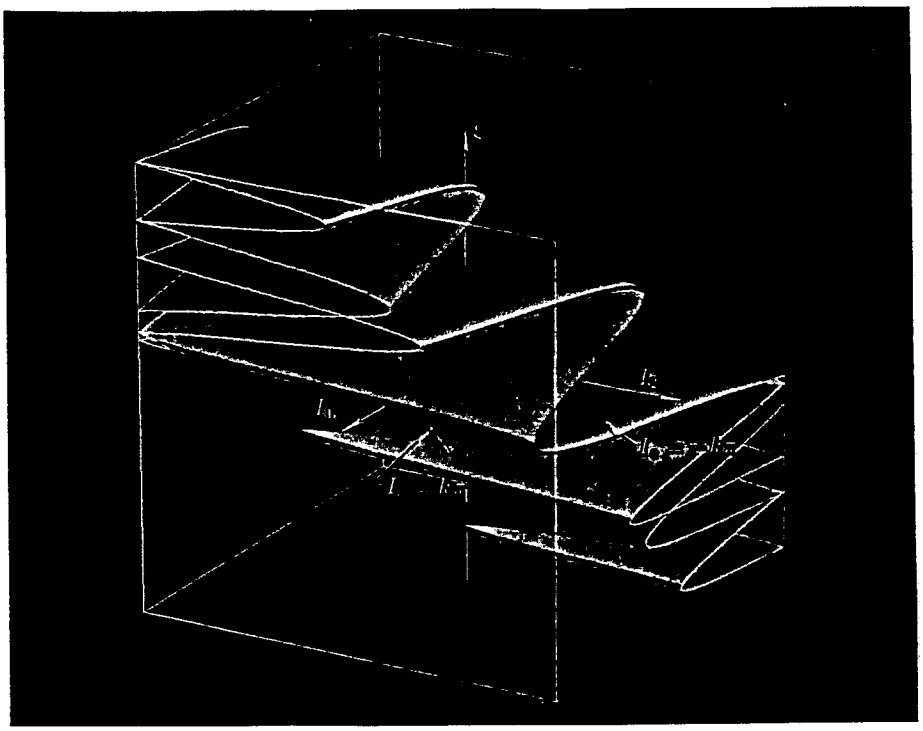

Fig. 3a

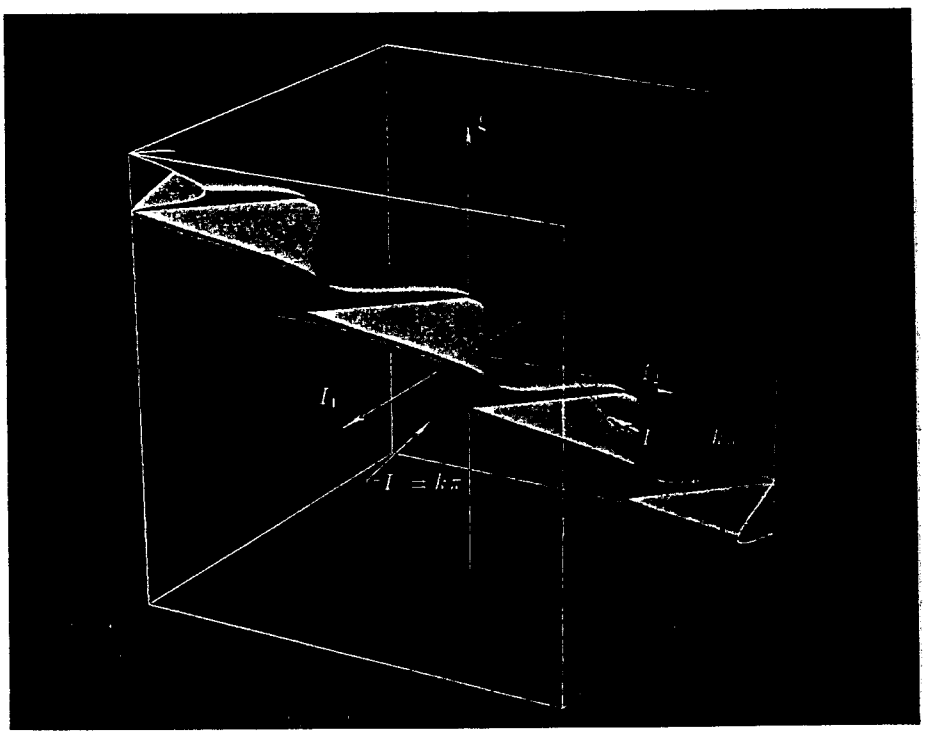

Fig. 3b

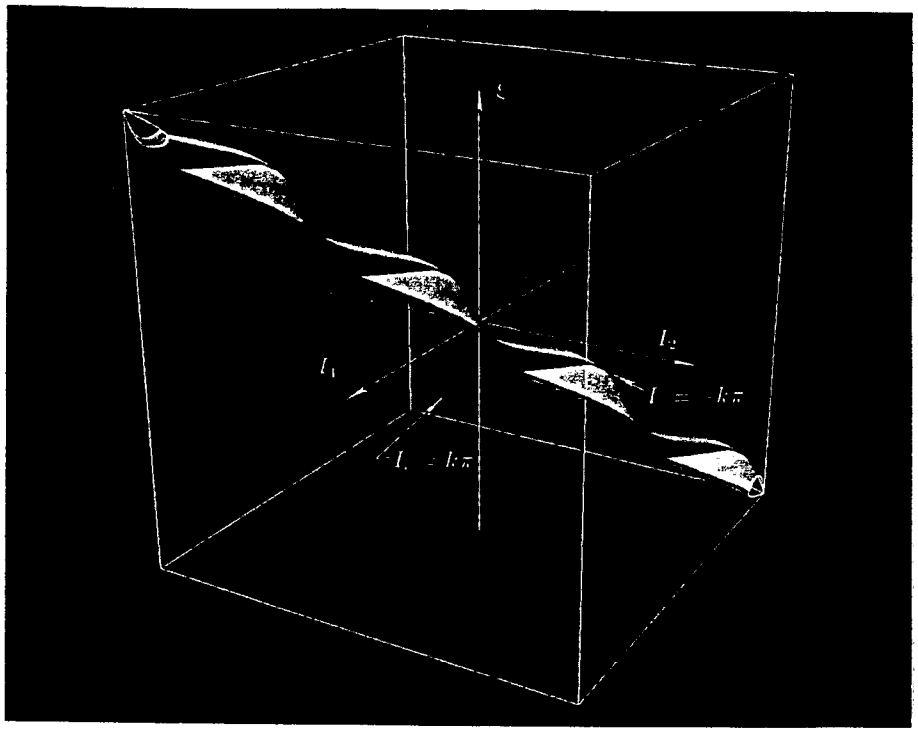

Fig. 3c

Fig. 3. The equilibrium points of the coupled pendula as a function of the applied torques I_1 and I_2, (a) for $k = 0.1$, (b) $k = 0.3$, and (c) $k = 0.6$. The vertical axis is the separation ξ of the pendula at the equilibrium. The colors correspond to the stability. White is stable, yellow is unstable. Red corresponds to $\rho > 0$ (see Sec. 3.1). Several images of the fundamental wedge are shown.

2.2.3. *Degenerate equilibrium points*

It is convenient to summarize the properties of the equilibrium points by the bifurcation set in the three-dimensional parameter space $\{(I_1, I_2, k)\}$. The sets corresponding to degenerate equilibrium points subdivide the parameter space into regions where the number and type of equilibrium points is constant.

Degenerate equilibrium points are determined by the condition that

$$\det \begin{pmatrix} \cos\phi_1 + k & -k \\ -k & \cos\phi_2 + k \end{pmatrix} = 0 ,$$

and thus they satisfy

$$\cos\phi_2 = -k\cos\phi_1/(\cos\phi_1 + k)$$

$$\sin\phi_1 + k(\phi_1 - \phi_2) = I_1$$

$$\sin\phi_2 + k(\phi_2 - \phi_1) = I_2 . \qquad (2.9)$$

Figure 4 shows the degenerate equilibrium points corresponding to Fig. 3a, and Fig. 5 shows the degenerate set in the three-dimensional parameter space.

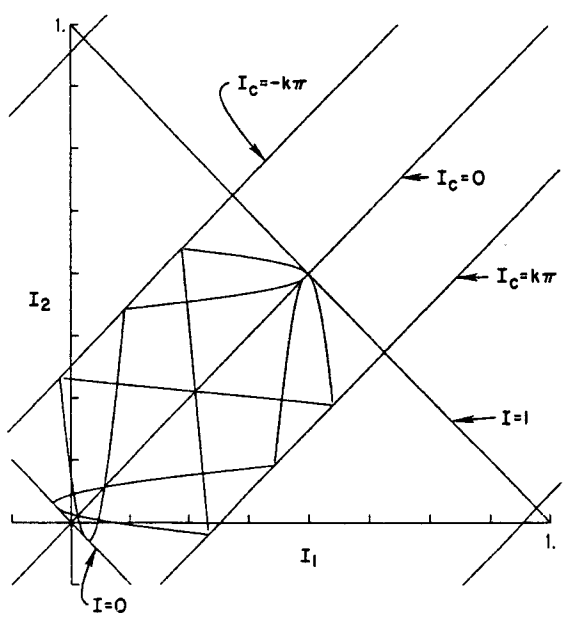

Fig. 4. The bifurcation set of equilibrium points at $k = 0.1$. The section of the fundamental wedge is marked, as is the line $I = 1$, above which no equilibrium points exist.

2.2.4. *Bifurcations of equilibrium points*

The condition for a degenerate equilibrium point is simply $ab = k^2$ (recall that $a = \cos\phi_1 + k$, $b = \sin\phi_2 + k$), so at the degenerate equilibrium points

$$\alpha_0 = 0, \quad \alpha_1 = -(a+b), \quad \text{if} \quad a+b>0\ ,$$

$$\alpha_0 = -(a+b), \quad \alpha_1 = 0, \quad \text{if} \quad a+b<0\ .$$

This implies that the null vector is

$a + b > 0$:

$$\lambda_{00} = 0\ ,$$
$$\lambda_{10} = -\gamma\ ,$$
$$\lambda_{01} = -\gamma/2 + \sqrt{\gamma^2/4 - (a+b)}\ ,$$
$$\lambda_{11} = -\gamma/2 - \sqrt{\gamma^2/4 - (a+b)}\ .$$

$a + b < 0$:

$$\lambda_{00} = -\gamma/2 + \sqrt{\gamma^2/4 - (a+b)}\ ,$$
$$\lambda_{10} = -\gamma/2 - \sqrt{\gamma^2/4 - (a+b)}\ ,$$
$$\lambda_{01} = 0\ ,$$
$$\lambda_{11} = -\gamma\ .$$

There are three possibilities as we move away from the equilibrium point:

1. If $\gamma^2/4 - (a+b) < 0$, the degenerate equilibrium point breaks into a stable node and a hyperbolic equilibrium point which has one unstable eigenvalue, one real stable eigenvalue, and a pair of complex stable eigenvalues.
2. If $0 < \gamma^2/4 - (a+b) < \gamma^2/4$, the degenerate equilibrium point breaks into a stable node and a hyperbolic equilibrium point which has one unstable and three real stable eigenvalues.
3. If $\gamma^2/4 < \gamma^2/4 - (a+b)$, the degenerate equilibrium point breaks into two hyperbolic equilibrium points, one which has two unstable and two real stable eigenvalues, and another with one unstable and three real stable eigenvalues.

2.3. *Periodic solutions*

From a computational standpoint, to understand the motions of the pendula we need to be able to compute periodic solutions of (1.1) and their dependence on the parameters. There are basically two approaches, the first is to integrate the equations numerically. With appropriate initial conditions, this allows the stable periodic solutions to be found. The second approach is to formulate a nonsingular, boundary-value problem for the periodic motions [Doedel *et al.*, 1984; Holodiniok & Kubiček, 1984; Keller & Jepson, 1984; and others] and to solve it using an iterative solver. This second approach has the advantage that both the stable and unstable motions are obtained, and that the period is explicitly computed.

The two-point, boundary-value problem for (1.1) with periodic boundary conditions is singular, with a null vector which (for autonomous systems) is simply the time derivative of the periodic solution. This singularity, which corresponds to an arbitrary shift in the origin of time, is removed by appending a phase constraint. As long as the phase constraint is not degenerate, this augmented system is regular for nonsingular periodic solutions.

We have used this approach with pseudo-arclength continuation [Keller, 1977], and computed all of the periodic solutions which are connected to the synchronous solution.

2.3.1. *Every nonequilibrium periodic solution is a running periodic solution*

Equation (2.3) is invariant under translations $\eta \to \eta + 2\pi$. By identifying the phase plane $(\xi, \eta, \dot\xi, \dot\eta)$ modulo this translation, we obtain a phase flow defined by (2.3) on the *cylinder* $S^1 \times \mathbb{R}^3 = \{(\xi, \eta \bmod 2\pi, \dot\xi, \dot\eta)\}$. Those periodic solutions which wind around the cylinder will be called "running" periodic solutions. For such solutions, we have $\eta(T) - \eta(0) = 2\pi m$ for some integer $m \neq 0$. We point out that *any periodic solution which is not an equilibrium is a running periodic solution.* In other words, any periodic solution with $\eta(t)$ bounded is actually an equilibrium. Indeed, for any periodic solution of period T with $\eta(T) - \eta(0) = 2\pi m$ we have

$$H(T) - H(0) = -2\pi m I = -\gamma \int_0^T (\dot\phi_1^2 + \dot\phi_2^2)dt\ ;$$

where the expression for H in the (ξ, η) variables was used in the first equality and the dissipation relation (2.2) in the second. This shows that $m \neq 0$, thus proving the remark.

2.3.2. *Discretization of the equations for periodic solutions*

To compute running periodic solutions, we introduce two 2π-periodic functions, p_1 and p_2. A running periodic solution of type m and period T is written as

$$\phi_1(t) = p_1(\omega t) + m\omega t$$
$$\phi_2(t) = p_2(\omega t) + m\omega t \qquad (2.10)$$

where $\omega = 2\pi/T$. A direct substitution gives the following equations for p_1 and p_2.

$$\omega^2 \ddot{p}_1 + \gamma\omega\dot{p}_1 + \sin(p_1 + \omega t) + k(p_1 - p_2) = I_1 - m\gamma\omega$$
$$\omega^2 \ddot{p}_2 + \gamma\omega\dot{p}_2 + \sin(p_2 + \omega t) + k(p_2 - p_1) = I_2 - m\gamma\omega \ . \qquad (2.11)$$

We approximate these equations on a uniform mesh in time using the second-order finite difference scheme:

$$\tilde{L}p_1 + \frac{1}{4}(E^2 + 2E + I)k(p_1 - p_2) = I_1 - m\omega$$
$$\tilde{L}p_2 + \frac{1}{4}(E^2 + 2E + I)k(p_2 - p_1) = I_2 - m\omega \qquad (2.12)$$

where

$$\tilde{L}u = \frac{\omega^2}{\Delta t^2}(E^2 - 2E + I)u + \frac{\gamma\omega}{2\Delta t}(E^2 - I)u + \frac{1}{4}(E^2 + 2E + I)\sin(u + \omega t) \ .$$

Here $Eu(t) = u(t + \Delta t)$ is the forward shift operator. This is equivalent to writing (2.12) as a first-order system $\dot{u} = f(u, t)$ and using the box scheme $(E - I)u/\Delta t = (E + I)f(u, t)/2$.

For general systems, it is best to use a phase constraint which approximately minimizes the L_2 norm of the derivative of the solution with respect to the parameter [Doedel *et al.*, 1984]:

$$\dot{x}_0^*(x - x_0) = 0.$$

We have also used the phase constraint

$$\phi_1(0) + \phi_2(0) = \eta(0) = 0 \ ,$$

originally for comparison with previous results. In practice, we experience no difficulties due to the possibly degenerate phase constraint, but do not recommend its use. The resulting system, boundary-value problem and phase constraint, can be viewed as a system for (ϕ_1, ϕ_2, T) as a function of (k, γ, I_1, I_2).

It is also possible to construct a system which allows homoclinic solutions to be computed directly [Beyn, 1987; Doedel & Friedman, 1989]. The system is constructed in the same manner as for a periodic solution, except that the boundary conditions are that as $t \to -\infty$ the solution approaches the equilibrium point along the unstable manifold of the equilibrium point, and as $t \to \infty$ it again approaches along the stable manifold. A phase constraint is again required.

2.3.3. *Continuation*

The basic computational task of the continuation method is the solution of linear systems involving the Jacobian. The Jacobian of this system, with the phase and arclength constraints, is a block tridiagonal matrix (with 4×4 blocks) bordered by six columns (four boundary values, the period and the parameter) and six rows (four for the periodic boundary conditions, the phase constraint and the pseudo-arclength constraint). On a mesh of N intervals this is an $(2N + 2) \times (2N + 2)$ system. We solve these systems using a bordering algorithm [Keller, 1977], which blocks the system into the form

$$\begin{pmatrix} A & b \\ c^* & d \end{pmatrix}$$

where A is a $(2N - 2) \times (2N - 2)$ block tridiagonal matrix, b and c are $(2N - 2) \times 4$ matrices, and d is a 4×4 matrix. The system can be solved using one LU factorization of A, and 5 backsolves.

Approximate Floquet multipliers may be found during the bordering algorithm by performing an eigenvalue decomposition of an intermediate 4×4 system. This requires two additional backsolves. For accuracy, we first eliminate the multiplier which sits at 1, using the phase constraint.

Bifurcation points are detected using the approximate Floquet multipliers. When a multiplier crosses the unit circle, a bisection algorithm is invoked to locate the precise point where it crosses. The eigenvector corresponding to this multiplier is then computed. (Using the intermediates of the bordering algorithm, this requires one backsolve.) This allows the tangent of the bifurcating branches at period-doubling and symmetry-breaking bifurcations to be computed. For example, if $u(t)$ is a running periodic solution of type m, and is a period-doubling bifurcation point, then the doubled branch is a running solution of type $2m$, and the doubled branch is approximately

$$\tilde{u}(t) \sim \begin{cases} u(t) + \varepsilon v(t) & 0 < t \le T \\ u(t) - \varepsilon v(t - T) & T < t \le 2T \end{cases}$$

where $v(t)$ is the eigenvector corresponding to the multiplier -1.

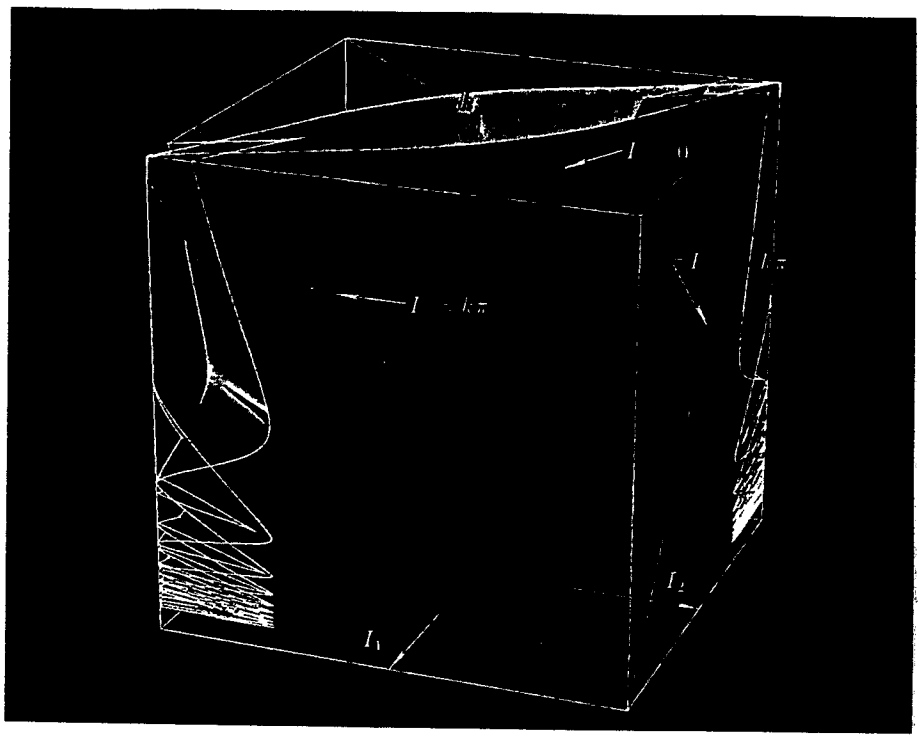

Fig. 5a. The bifurcation set of equilibrium points in the entire parameter space. Several images of the fundamental wedge are shown.

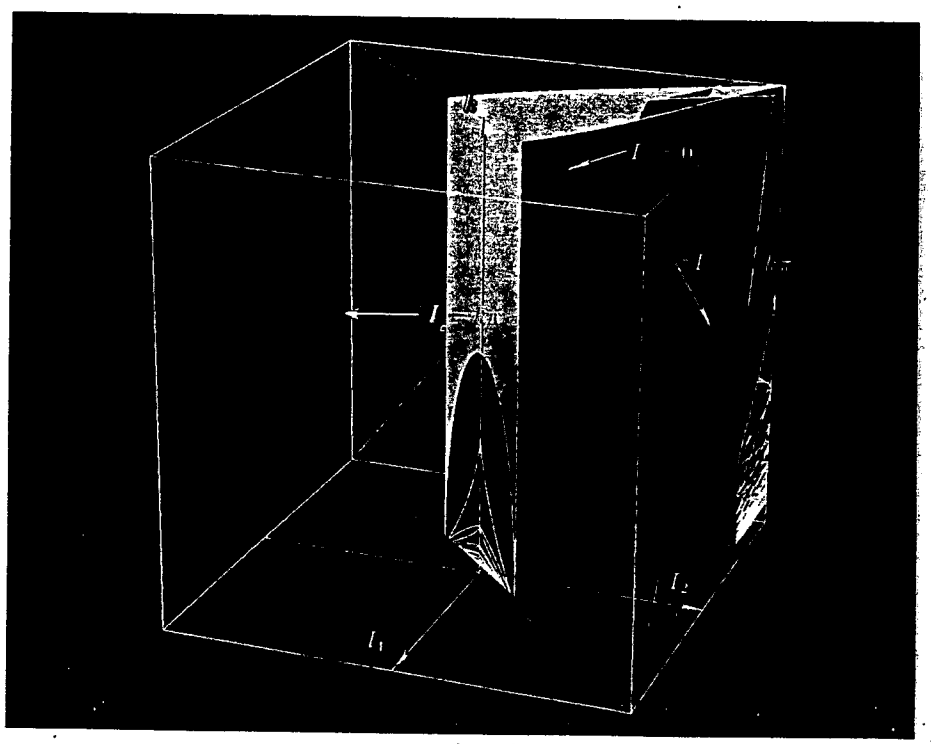

Fig. 5b. The interior of the bifurcation set shown in Fig. 5a.

There are two regimes for which asymptotic expressions for periodic solutions are known. These are strong ($k\gamma^2 \gg 1$) and weak coupling. The synchronous solution exists for strong coupling, and is such that the separation between the pendula is essentially constant over the period; hence the pendula move roughly as a single pendulum. The synchronous solution is given approximately by

$$\omega_s \sim I/\gamma ,$$
$$\eta_s \sim \omega t ,$$
$$\xi_s \sim I_c/2k .$$

The small coupling ('caterpillar') solutions have already been discussed (Sec. 1.2), but are rather more difficult to construct, and require a good adaptive mesh strategy to handle the different time scales during the period.

2.3.4. *Nonexistence of quasiperiodic and torus bifurcations*

The damped Hamiltonian structure drastically simplifies the possible bifurcation behavior of periodic solutions. The following result is the dissipative Hamiltonian version of the Lyapunov–Poincaré theorem [Yakubovick & Starzhinskii, 1975].

Theorem 2.1.[1] *Let $x(t)$ be a periodic trajectory of the damped Hamiltonian system (2.1) with period T. Then Floquet multipliers of $x(t)$ must appear in quadruplets $(\mu, \bar{\mu}, e^{-\gamma T}/\mu, e^{-\gamma T}/\bar{\mu})$.*

Proof: The linearization of (2.1) about the periodic trajectory $x(t)$ is

$$\dot{\mathbf{y}} = (JH''(t) - \gamma D)\,\mathbf{y} ,$$

where H'' is the Hessian matrix of H:

$$H''_{ij}(t) = \left.\frac{\partial^2 H}{\partial x_i \partial x_j}\right|_{x(t)} .$$

The fundamental solution matrix Y of this equation is defined by

$$\dot{Y} = (JH''(t) - \gamma D)Y, \qquad Y(0) = I .$$

A simple substitution shows that the product Y^TJY, satisfies

$$\frac{d}{dt}(Y^TJY) = -\gamma(Y^TJY) ,$$

which implies the "dissipative symplectic" character of Y:

$$Y^TJY = e^{-\gamma t}J .$$

Thus $e^{(1/2)\gamma t}Y(t)$ is symplectic ($(e^{(1/2)\gamma t}Y)^TJ(e^{(1/2)\gamma t}Y) = J$), and its eigenvalues appear in quadruplets of the form $(\lambda, \bar{\lambda}, 1/\lambda, 1/\bar{\lambda})$. The Floquet multipliers of the trajectory are the eigenvalues of $Y(T)$.

This result drastically simplifies the possible bifurcation behavior on periodic solution branches of (1.1). If $x(t)$ is a periodic motion of period T, one of its Floquet multipliers is 1. There are only two possibilities for the set of Floquet multipliers:

$$\left(1, e^{-\gamma T}, \alpha e^{-(1/2)\gamma T}, \frac{1}{\alpha} e^{-(1/2)\gamma T}\right), \quad \alpha \in \mathbb{R}$$

or

$$(1, e^{-\gamma T}, \beta e^{-(1/2)\gamma T}, \bar{\beta} e^{-(1/2)\gamma T}), \qquad \beta \in \mathbb{C}, \quad |\beta| = 1 .$$

A bifurcation occurs on a periodic branch when one or more Floquet multipliers lie on the unit circle. This crossing can happen only at ± 1, (for $\alpha = \pm e^{(1/2)\gamma T}$), and only one multiplier can cross. This means that only regular and period-doubling bifurcations can occur.

3. Geometry of Shil'nikov's bifurcations

We give a brief exposition of the essential part of Shil'nikov's picture [Ovsyannikov & Shil'nikov, 1987] which allows one to visualize at a glance all the consequences of a homoclinic saddle-focus connection. Full details and proofs can be found in Ovsyannikov & Shil'nikov [1987]; see also Glendinning & Sparrow [1984] for a discussion of the three-dimensional case.

3.1. *Poincaré map and its properties*

Consider a flow in $\mathbb{R}^4$ with a saddle-focus equilibrium,[2] i.e., let the eigenvalues satisfy $\lambda_{1,2} = \alpha \pm i\omega$, $\omega \neq 0$, $\lambda_3 < \alpha < 0$, $\lambda_4 > -\alpha (> 0)$. Without loss of generality, we assume the equilibrium to be at the origin with the x_1, x_2-plane being the eigenplane of $\lambda_{1,2}$ and with x_3-, x_4-axes being the eigendirections of λ_3, λ_4 correspondingly (Fig. 6).

[1] The version of the proof given here is due to L. Reyna, IBM Research.
[2] Consideration of a flow in $\mathbb{R}^4$ poses a difficulty not present in $\mathbb{R}^3$. Taking a dimension higher than 4, on the other hand, adds no new problems.

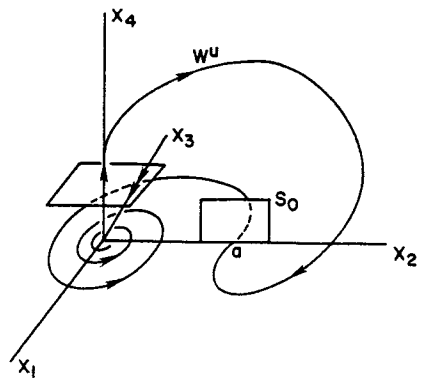

Fig. 6. The saddle-focus equilibrium and homoclinic connection.

Let W^u be the unstable manifold of the saddle-focus; we assume a homoclinic connection, i.e., we assume that the solutions lying on W^u approach the saddle-focus for $t \to +\infty$ as well. Without loss of generality, we assume that the flow is linear in a δ-neighborhood N_δ ($\delta > 0$) of the origin. Choosing a point $\mathbf{a} = (0, a, x_3^0, 0) \in N_\delta \cap W^u \cap W^s$ at a distance $\leq \frac{\delta}{2}$ from the origin (Fig. 6), we define the Poincaré section S_0 by

$$\begin{cases} x_1 = 0 \\ a/2 < x_2 < \delta \\ -\delta \leq x_3 \leq \delta \\ 0 \leq x_4 \leq \delta \end{cases}.$$

We define another section S_1 by $S_1 = \{x_4 = \delta,\ |x_1| + |x_2| + |x_3| \leq \delta\}$, and introduce the section maps F_{01} and F_{10} from S_0 to S_1 and from S_1 to S_0 by following the flow from one section to another. The map F_{01} can easily be written out explicitly using the linearity of the flow near the origin:

$$F_{01}: \begin{pmatrix} 0 \\ x_2 \\ x_3 \\ x_4 \end{pmatrix} \to \begin{pmatrix} -x_2 e^{\alpha t} \sin \omega t \\ x_2 e^{\alpha t} \cos \omega t \\ x_3 e^{\lambda_3 t} \\ \delta \end{pmatrix} = \begin{pmatrix} x_1' \\ x_2' \\ x_3' \\ x_4' \end{pmatrix},$$

where

$$t = \frac{1}{\lambda_4} \ln \frac{\delta}{x_4},$$

or more explicitly, with $\rho = \frac{-\alpha}{\lambda_4}$,

$$x_1' = -x_2 \left(\frac{x_4}{\delta}\right)^{\rho} \sin\left(\frac{\omega}{\lambda_4} \ln \frac{\delta}{x_4}\right),$$

$$x_2' = -x_2 \left(\frac{x_4}{\delta}\right)^{\rho} \cos\left(\frac{\omega}{\lambda_4} \ln \frac{\delta}{x_4}\right),$$

$$x_3' = -x_3 \left(\frac{x_4}{\delta}\right)^{\rho_+},$$

where $\rho_+ = \frac{-\lambda_3}{\lambda_4} > \rho$. The expression for F_{10} depends on the global behavior of W^u; in a neighborhood of $(0, 0, 0, \delta)$ it can be approximated by a linear map

$$F_{10}: \begin{pmatrix} x_1 \\ x_2 \\ x_3 \\ \delta \end{pmatrix} \to \mathbf{a} + A \begin{pmatrix} x_1 \\ x_2 \\ x_3 \end{pmatrix} = \begin{pmatrix} x_1'' \\ x_2'' \\ x_3'' \\ x_4'' \end{pmatrix}$$

where A is a 4×3 matrix determined by the linearization of the flow along the piece of W^u joining S_1 to S_0.

The composition $F = F_{10} \circ F_{01}$ taking S_0 to itself [3] is shown in Fig. 7.

We note first that the image $F_{01}S_0$ is close to the 2-dimensional (x_1, x_2)-plane in the three-dimensional section S_1, since the x_3-coordinates of the images are small compared to the other two: $e^{\gamma_3 t} \ll e^{\alpha t}$.

The image $F_{01}S_0$ looks like a spiral; horizontal slices $x_4 = \text{const.}$ of S_0 map into transversal sections of the spiral, as shown in Fig. 7; as x_4 decreases to 0, thesections zoom around the spiral infinitely many times, tending to the center.

The *tightness* of the spiral is determined by the ratio $\rho = \frac{-\alpha}{\lambda_4}$: if $\rho < 1$, the spiral is tight on the outside and "sparse" closer to its center (Fig. 8) while $\rho > 1$ the opposite is the case. One might restate this even more loosely by saying that for $\rho < 1$ a passage by the hyperbolic equilibrium in the phase plane has a stretching effect, while for $\rho > 1$ the effect is a compression.

The map F_{10} takes the nearly two-dimensional spiral affinely into the cube S_0, as shown in Fig. 7; we want to avoid the possibility of having the image in S_0 of the two-dimensional tangent plane (at the center) of the spiral to be of dimension one. Subject to this transversality condition, the image $(F_{10} \circ F_{01})S_0$ is a spiral as shown in Fig. 8.

We now assume that with an extra parameter b we can move the unstable manifold W^u so that the x_4-coordinate of the intersection $W^u \cap S_0$ (which is the center of the spiral) changes together with b. The vertical (x_4) position of the center of the spiral will

[3] F_{01} may be undefined on parts of S_0.

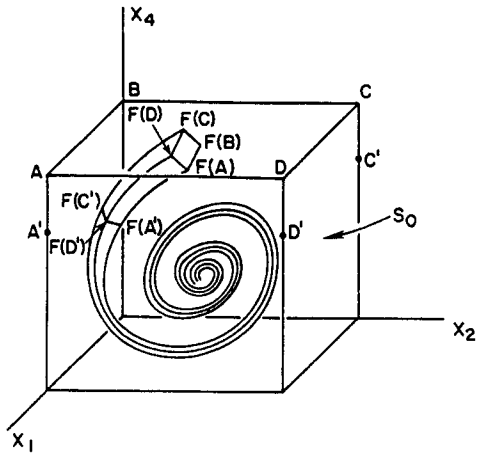

Fig. 7 The section S_0 and the image of a cube under F, which maps S_0 into itself.

have an effect on the qualitative properties of the map. It is not necessary to introduce a second parameter controlling the horizontal position of the spiral's center since horizontal sections $x_4 = \text{const.}$ of the cube S_0 have small images for small x_4.

As observed above, the map F is nearly two-dimensional: the image of S_0 in S_0 lies in a small (with respect to δ) neighborhood of a 2-D plane.

Approximating this 3-D map by a 2-D map, we reduce the problem to a mapping of the plane to itself, as shown in Fig. 8. This can be done rigorously. The resulting map can be further reduced to a one-dimensional map $x_4 \mapsto f(x_4)$ with little loss of information, by assigning the x_4-coordinate $f(x_4)$ to the point $(x_1 = 0, x_2 = a, x_3 = 0, x_4)$.

As the parameter b changes, the graph of f shown in Fig. 8 moves in a vertical direction with saddle-node pairs of equilibrium points of the map f appearing or disappearing each time the graph becomes tangent to the bisector.

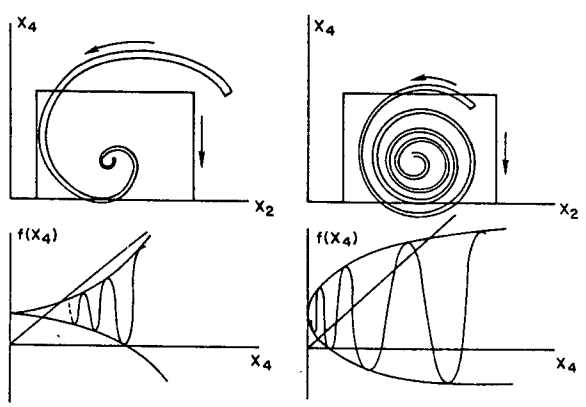

Fig. 8. The spiral for $\rho < 1$ (left) and $\rho > 1$ (right). Below each spiral is the corresponding map $f(X_4)$.

4. Existence of Homoclinic and Heteroclinic Connections

In this section, we prove the existence of homoclinic and heteroclinic connections for the system of coupled pendula. The theorem below states the existence of homoclinic connections for moderate values of k. Numerical evidence presented in the following section shows the existence of homoclinic connections with fewer restrictions on the parameters.

Theorem 4.1. *Let k be such that, for all I_1, I_2, there exist exactly two equilibria for*

$$\begin{cases} L\phi_1 + k(\phi_1 - \phi_2) = I_1 \\ L\phi_2 + k(\phi_2 - \phi_1) = I_2 \end{cases} \tag{4.1}$$

where $L\phi = \ddot{\phi} + \gamma\dot{\phi} + \sin\phi$. (Any $k > 1$, for instance, satisfies this condition.) For any fixed value of I_1, there exists a corresponding value $I_2 = I_2(I_1, k, \gamma)$ with $0 < I_1 + I_2 < 2$ such that Eq. (4.1) possesses a homoclinic solution connecting the (unique) saddle to itself.

Proof. The two equilibria of the pendula are sketched in Fig. 9 below.

Let $\Phi(t) \equiv \Phi(t, I_1, I_2) \equiv (\phi_1, \phi_2, \dot{\phi}_1, \dot{\phi}_2)$ be a solution lying on the unstable manifold W^u of the saddle, with $\xi > 0$. We note that $\Phi(t)$ is defined uniquely up to a time-translation. Fixing any arbitary value of I_1 throughout this argument, we follow the behavior of the unstable manifold $\Phi(t, I_1, I_2) \equiv \Phi(t, I_2)$ for different values of I_2.

For $I_1 + I_2 = 0$, any solution, and in particular $\Phi(t)$, tends to a sink. Let I_2^* be the largest number such that for all $-I_1 < I_2 < I_1$ the unstable manifold solution $\Phi(t, I_2)$ terminates in the sink. It is clear that $I_2^* + I_1 > 0$, since the property of terminating in the sink is an open one. We would like to prove that $I_2 = I_2^*$ is the homoclinic value; to that end, it suffices to show that $\Phi(t, I_2^*)$ tends to an equilibrium; by the definition of I_2^*, it must be a saddle, which prove the theorem. To prove that the solution $\Phi(t, I_2^*)$ does indeed tend to an equilibrium, we show first that the number of tumbles (of the center of mass η of the solutions $\Phi(t, I_2)$) is bounded uniformly for all

$$-I_1 \le I_2 < I_2^* ; \tag{4.2}$$

more precisely, we will show that there exists a constant bound $B > 0$ such that for all I_2 in the interval (4.2) we have

$$\eta(t) - \eta(-\infty) \equiv \frac{1}{2}(\phi_1 + \phi_2)\Big|_{-\infty}^{t} \le B \tag{4.3}$$

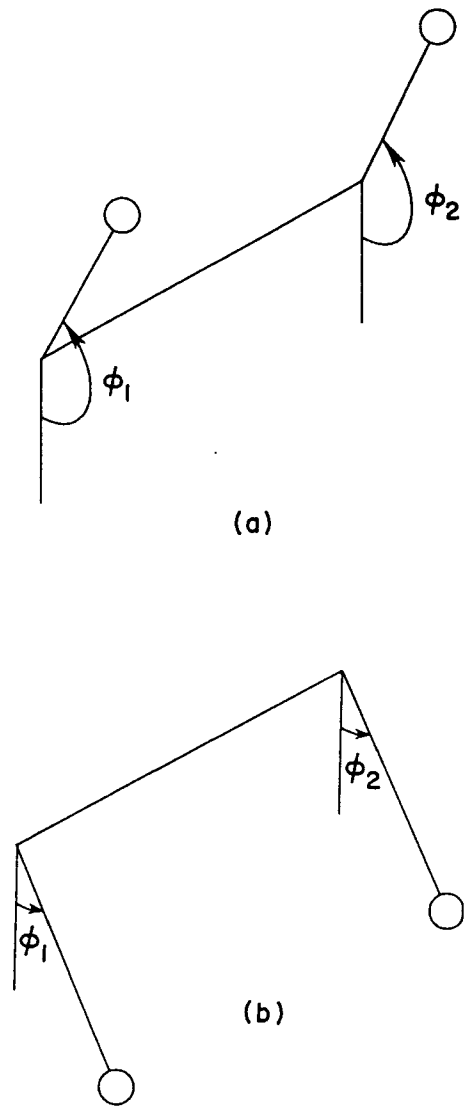

Fig. 9. The two equilibria of Theorem 4.1.

for all $t \in (-\infty, \infty)$.

We first prove this bound, and then use it to show that $I_2 = I_2^*$ is indeed the homoclinic value. The Hamiltonian

$$H = \frac{1}{2}(\dot{\xi}^2 + \dot{\eta}^2) + k\xi^2 - I_c\xi - \cos\eta\cos\xi - I\eta$$

is decreasing along any solution, so that for any t we have

$$H(t) \geq H(\infty) \ . \tag{4.4}$$

To estimate $H(\infty)$ we note that for any I_2 subject to (4.2) the statements (i)–(iii) hold:

(i) $\dot{\xi}(\infty) = \dot{\eta}(\infty) = 0$; any equilibrium satisfies

(ii) $|\xi(\infty)| < \frac{|I_2 - I_1|/2 + 1}{k}$, and

(iii) there exists a constant $A > 0$ such that $|\eta(\infty)| < A$.

Indeed, (i) follows from the fact that each solution on W^u tends to an equilibrium for $-I_1 < I_2 < I_2^*$. The bound (ii) on $|\xi(\infty)|$ is obvious from the equilibrium equations (2.7). To prove (iii) we note that $\eta(t, I_2)$ is continuous in I_2 and its limit $\eta(\infty, I_2)$ is at the sink for each value of I_2 in the interval (4.2), and therefore S is continuous in I_2 in the interval (4.2) and consequently stays bounded as $I_2 \to I_2^*$. It should be pointed out that no statement is made (as yet) about the boundedness of $\eta(t)$ uniformly in t and I_2, but only about the limit $\eta(\infty, I_2)$, uniformly in I_2. Using these estimates, we conclude that

$$H(\infty) \geq C(k, A) \ , \tag{4.5}$$

for all I_2 in the interval (4.2). We also note that there exists a bound C uniform in I_2 lying in any bounded interval (and in (4.2) in particular):

$$|\xi|, |\dot{\xi}|, |\dot{\eta}| < C \quad \forall t \in \mathbb{R} \ , \tag{4.6}$$

as has been shown by a Lyapunov function argument [Levi *et al.*, 1978]. Using these bounds we obtain from Eqs. (4.4) and (4.5):

$$\eta(t) \leq \frac{1}{I}\Big(-H(\infty) + \frac{1}{2}(\dot{\xi}^2 + \dot{\eta}^2) + 2k\xi^2 - 2K\xi - 2\cos\eta\cos\xi \Big) < \frac{1}{I}(C^2(1 + 2k) + 2KC + 2) \equiv B \ .$$

Having thus established the key bound (4.3) we show that $I = I_2^*$ is a homoclinic value. Indeed, $\Phi(t, I_2^*)$ is bounded: for $I = I_2^*$ the estimate (4.3) still holds by continuity of $\eta(t, I_2)$ in I_2: we take the limit as $I_2 \to I_2^*$ for each fixed t.

We conclude from the boundedness of the sum $2\eta = \phi_1(t, I_2^*) + \phi_2(t, I_2^*)$ that $\Phi(t, I_2^*)$ tends to an equilibrium. This equilibrium cannot be a sink, since otherwise I_2^* could be increased further, contrary to its definition. Hence $\Phi(t, I_2^*)$ tends to the saddle, which completes the proof.

Remark. If k is small enough, there exist no heteroclinic loops, i.e., connections of the type $A - B - A$ between any two saddle points A and B. We do not carry out the details, but only mention that this can be proved by treating each equation in the system as an

equation of a single pendulum with a *slowly varying* torque, by the approach used in Levi [1988]. This slow variation precludes, as it turns out, a homoclinic connection $A \to B$ between two points A and B if there already exists a connection $B \to A$. This impossibility is due to the dissipation of inertial effects which occurs over a long relaxation time during which one pendulum moves and the other "stands".

5. Computational Results

5.1. *Periodic solutions connected to the synchronous solution*

The following results were obtained with a mesh of 250 points per period. For period-doubled branches, this was doubled to 500 points in order to preserve the overall accuracy of the solution. We found, by recomputing certain solutions with a finer mesh, that this mesh was sufficient except for the very long period solutions ($T > 50$), that is, the near-homoclinic solutions. For the results below, the approach to the homoclinic solution was sufficiently rapid that the correct location could be found well before the mesh became inadequate. The location of the homoclinic orbits at several points was checked with computations on a mesh with 180 points, and the results agree to one percent.

For fixed $k = 0.1$ and $\gamma = 0.5$, we find that there is a path of homoclinic orbits which extends from $I_c = 0$ to $I_c = k\pi$. There are two pairs of folds on this path, which break the interval into several pieces, corresponding to different behavior of the branch of periodic solutions connected to the synchronous solution.

For $0 \le I_c < 0.65k\pi$, the synchronous solution has increasing period as I is decreased (Fig. 10). The pendula each makes one 'tumble' per period, and they do this in unison. As I is decreased, the time between tumbles increases and the solutions on the branch approach the homoclinic orbit A. I_c controls the separation between the pendula, which is essentially constant over the period. As I_c approaches zero the homoclinic orbit A approaches the symmetric homoclinic orbit where the pendula act as a single pendulum. Near $I = 0.7$ the main branch undergoes a period-doubling bifurcation, which also breaks the synchronization between the pendula. The period-doubled branch initially increases in period as I increases, with one pendula tumbling slightly before the other. At larger $I < 1$, there is a fold on the doubled branch, after which the period increases as I decreases, eventually approaching the homoclinic orbit A'. This orbit is associated with a saddle-focus, and has a value of ρ near 0.3. The excursion of the branch to the fold point serves to move the periodic orbit away from the equilibrium point with small ξ and toward the saddle–focus.

Near $I_c = 0.525k\pi$, a second branch of periodic solutions appears (Fig. 11). This branch still consists of running periodic solutions with $m = 1$, and connects two homoclinic orbits B and C. As I_c is increased, this branch widens, until near $I_c = 0.675$ the homoclinic orbit B coalesces with the homoclinic orbit A on the main branch in a fold on the path of homoclinic orbits. Homoclinic orbits B and C each pass close to two equilibrium points, one of which is the equilibrium point associated with the homoclinic orbit A, the other is a saddle-focus. Homoclinic orbits B and C can be distinguished by how close they approach these equilibrium points. B spends roughly equal time near both equilibrium points, while C stays longer near the saddle-focus.

For $0.675k\pi \le I_c < 0.95k\pi$, the branch containing the synchronous solution approaches homoclinic orbit C in an oscillatory manner, consistent with the behavior near a Shil'nikov-type orbit with $\rho < 1$. We find that for the saddle-focus associated with orbit C, the parameter ρ is approximately 0.65 near $I_c = 0.95k\pi$, and decreases to about 0.5 as I_c approaches $0.675\ k\pi$. Between the folds on the periodic solution branch (e.g., a–a' in Fig. 12) lie pairs of period-doubling bifurcations. These occur where the analysis of the return map near the homoclinic orbit predicts that the main branch should lose stability (see Glendinning & Sparrow [1984]). The period-doubled branches emanating from the bifurcation points approach secondary homoclinic orbits D and E, and show the same oscillations that the main branch does. We have not checked the stability of these doubled branches, but it is likely that they also have pairs of period-doubling bifurcations, which lead to a second level of secondary homoclinic orbits. As I_c approaches $0.675k\pi$, the main branch develops a region with large period, which eventually forms the pair of homoclinic orbits AB discussed above.

For $0.95k\pi \le I_c \le k\pi$ the synchronous solution again approaches a homoclinic orbit (A) of the Shil'nikov type, with $\rho < 1$ (Fig. 13). There is again a disjoint branch connecting two homoclinic orbits (B and C). As I_c is decreased, B and A coalesce, leaving C to persist for lower values of I_c. The homoclinic orbits appear to be the large limits of the three branches of a perturbed symmetry-breaking bifurcation. The homoclinic orbits spend time near two equilibrium points with nearly the same value of η, but oppositely signed

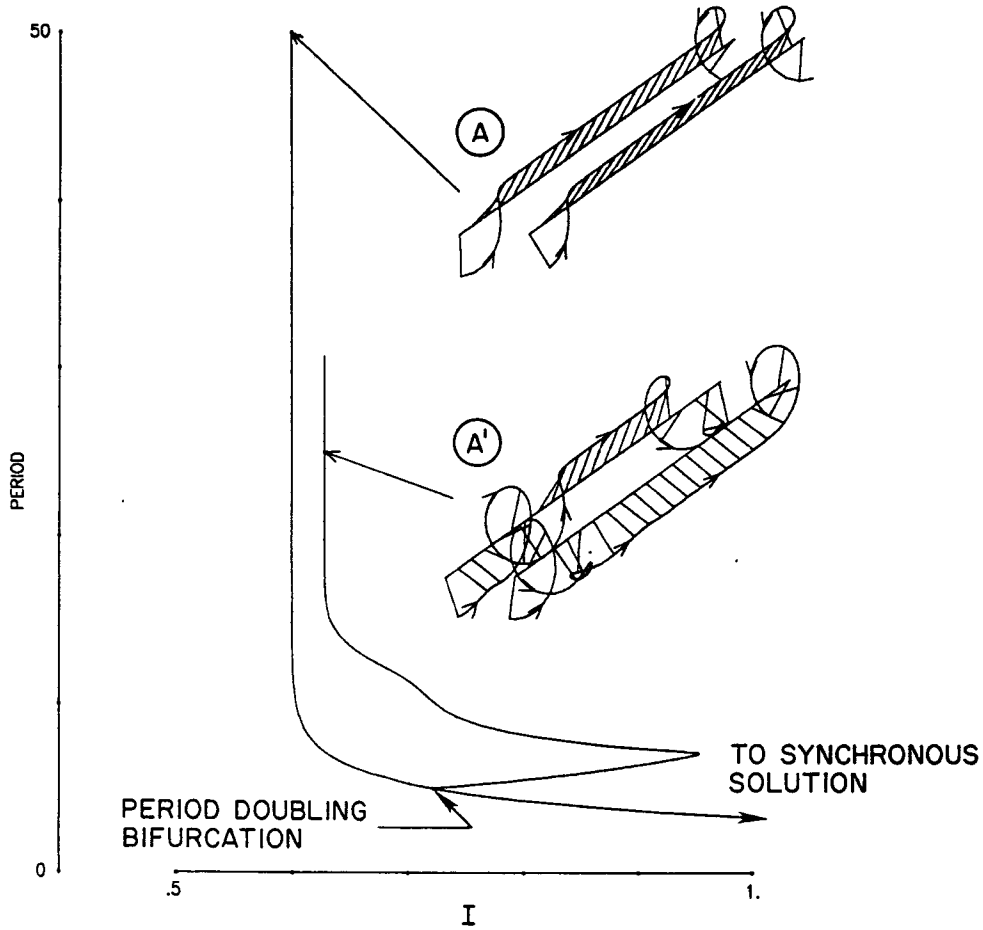

Fig. 10. The periodic solutions connected to the synchronous solution for $k = 0.1$, $\gamma = 0.5$, $I_c = 0.1k\pi$. Solutions were computed on a mesh of 250 points per period. Solution A is nearly homoclinic, with one tumble per period. Solution A′ is nearly homoclinic with two tumbles per period. The period shown for the period-doubled branch is half the actual period.

values of the separation ξ. Homoclinic orbit A spends more time near one equilibrium point than the other, C spends more time near the other, and orbit B spends roughly equal time near both.

5.2. *Paths of homoclinic solutions*

In Fig. 14 we show computed curves of homoclinic connections for $k = 0.1$ and $\gamma = 0.5$.

The behavior of the periodic orbits near the homoclinic connection associated with a saddle-focus is determined by ρ, the ratio of the strength of the stable focus to the strength of the unstable direction. Near a degenerate equilibrium point which breaks into a saddle and a stable focus

$$\rho = \frac{-\mathrm{Re}(\lambda_{01})}{\lambda_{00}} = \frac{\gamma/2}{-\gamma/2 + \sqrt{\frac{1}{4}\gamma^2 - \frac{1}{2}(a+b) + \sqrt{\frac{1}{4}(a-b)^2 + k^2}}}.$$

Near the degenerate point, ρ becomes infinitely large. The critical value is $\rho = 1$, which is determined by the condition that

$$\frac{1}{4}\gamma^2 - \frac{1}{2}(a+b) + \sqrt{\frac{1}{4}(a-b)^2 + k^2} = \gamma^2 .$$

Or,

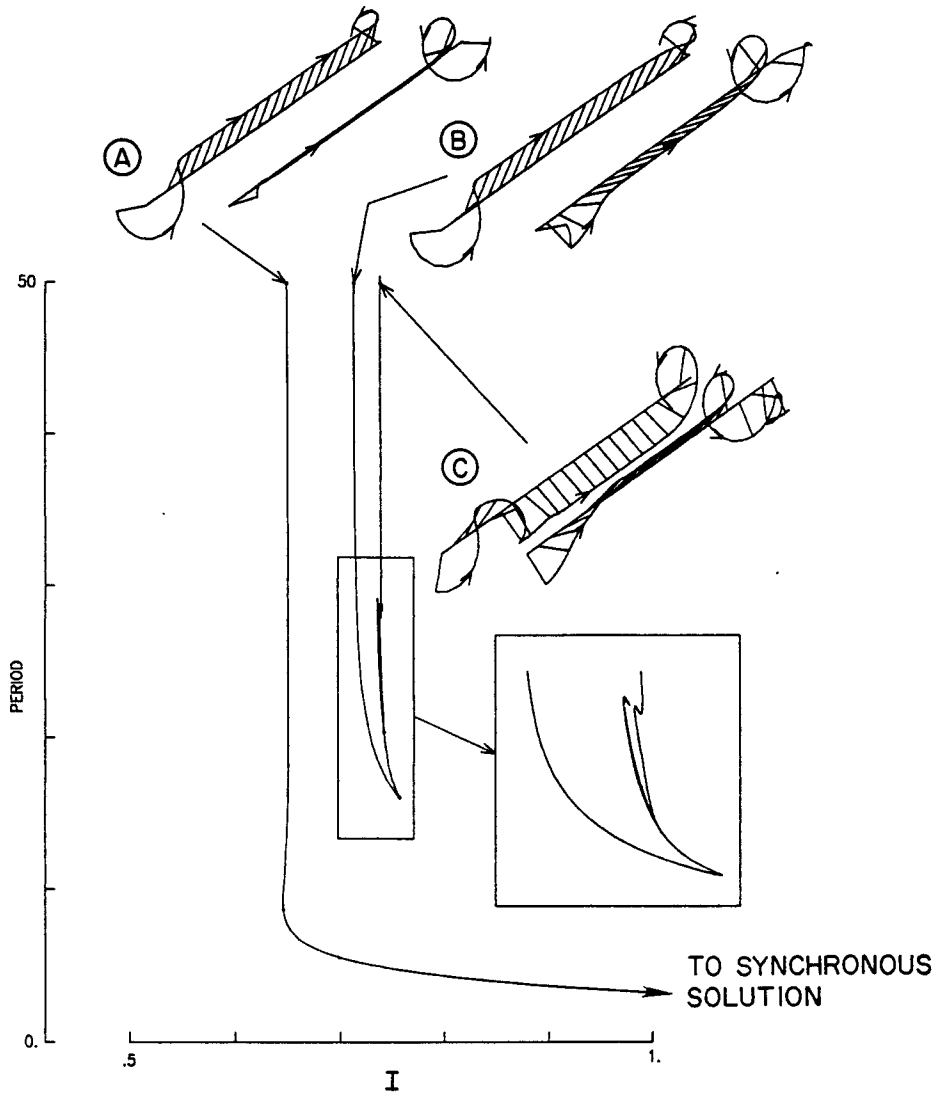

Fig. 11. The periodic solutions for $k = 0.1$, $\gamma = 0.5$, $I_c = 0.55k\pi$. A branch of period-doubled solutions also exists, but is not shown. (The mesh is the same as in Fig. 10).

$$\cos\phi_2 = \frac{-k\cos\phi_1 - \frac{3}{4}\gamma^2\left(\frac{3}{4}\gamma^2 + \cos\phi_1 + 2k\right)}{\cos\phi_1 + k + \frac{3}{4}\gamma^2}$$

$$I_1 = \sin\phi_1 + k(\phi_1 - \phi_2) \tag{5.1}$$

$$I_2 = \sin\phi_2 + k(\phi_2 - \phi_1)\ .$$

This is subject to the conditions that the equilibrium point be hyperbolic,

$$-\frac{1}{2}(a+b) + \sqrt{\frac{1}{4}(a-b)^2 + k^2} > 0$$

$$\frac{1}{4}\gamma^2 - \frac{1}{2}(a+b) - \sqrt{\frac{1}{4}(a-b)^2 + k^2} < 0\ .$$

As the damping γ goes to zero, these lines of $\rho = 1$ approach the lines of degenerate equilibrium points (compare (5.1) to (2.3)).

These critical lines are shown in Fig. 14, together with the paths of homoclinic connections. The curves of homoclinic orbits do not cross the critical lines. Homoclinic orbits on the lower branch of the "S" (A and B for $I_c < 0.675k\pi$) are not of the Shil'nikov type; branch C is, with values of ρ between 0.4 and 0.65.

6. Physical consequences of Shil'nikov's picture

After the existence of the saddle-focus connections has been established, it remains to interpret geometrical properties of Poincaré map in terms of the motions of the pendula.

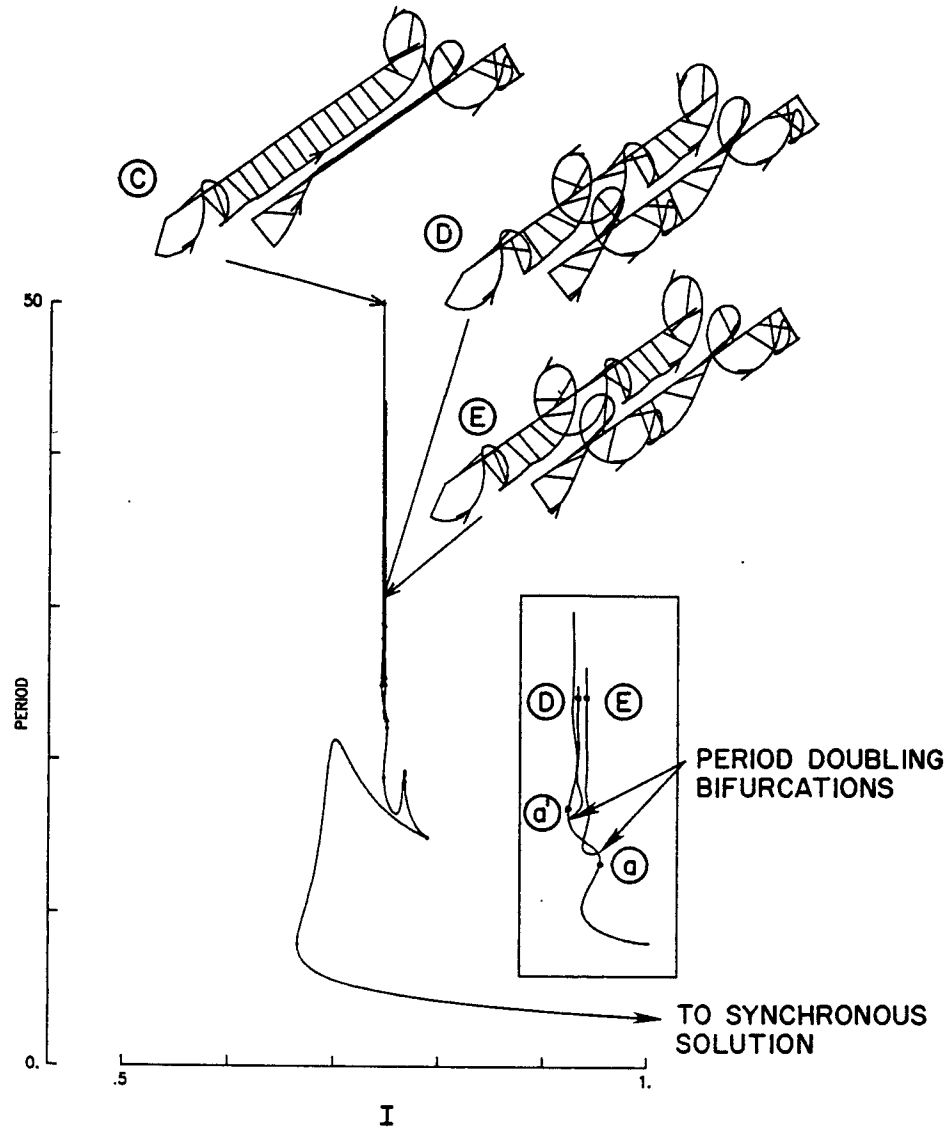

Fig. 12. The periodic solutions connected to the synchronous solutions for $k = 0.1$, $\gamma = 0.5$, $I_c = 0.675k\pi$. Points on the solution branches are quadratic fold points. (The mesh is the same as in Fig. 10).

We give here a translation of the geometry of the map into the physics of motion.

Referring to Fig. 7, let us move an initial condition $z \in S_0$ down towards the plane $x_4 = 0$. The image $F(z)$ will travel along the spiral towards its center, executing infinitely many revolutions.

One revolution of $F(z)$ along the spiral corresponds to the trajectory of the flow making one extra rotation in the (x_1, x_2)-plane; this in turn corresponds to the angle $(\phi_1 - \phi_2)$ between the pendula making one extra oscillation.

Using this key remark, we translate the result of the geometric discussion, obtaining the following consequences. For convenience, we fix I_c to be constant and choose I as the parameter.

1. There exists an integer N, and a countable set of parameter intervals $\mathbf{I}^n$ *enumerated by* $n > N$ such that, for each $I \in \mathbf{I}^n$, Eq. (1.1) has stable periodic solutions executing n relative oscillations of ξ for each full revolution of η.

The computations show this as an oscillation of the branch of periodic solutions as it approaches the homoclinic orbit. Figure 15 shows solutions for $I_c = 0.7k\pi$ at various points on the path; we sketch the orbit in the neighborhood of the saddle-focus as well as the corresponding physical motion of the pendula. Each fold on the solution path adds another oscillation about the equilibrium point, which is consistent with Fig. 13. At a fixed value of

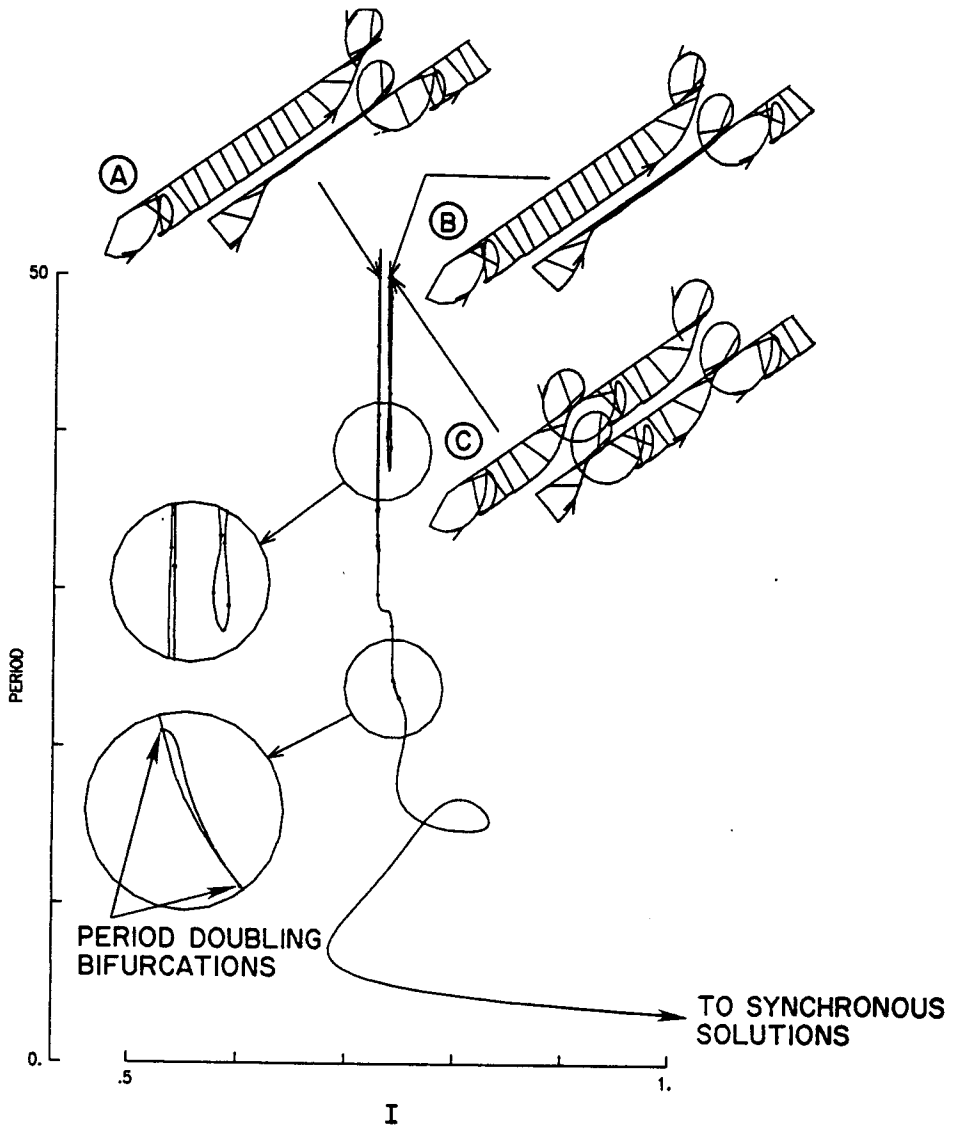

Fig. 13. The periodic solutions connected to the synchronous solution for $k = 0.1$, $\gamma = 0.5$, $I_c = 0.975k\pi$. (The mesh is the same as in Fig. 10).

I we see a sequence of fixed points of the return map with decreasing values of x_4 and increasing period.

2. For some (actually, for a Cantor set of) parameters the map possesses infinitely many coexisting sinks; Eq. (1.1) thus possesses infinitely many coexisting stable periodic solutions.
3. In the near-homoclinic case and for $\rho > 1$, Eq. (1.1) possesses a small attractor (in the sense of Conley [1978]), which is either a stable periodic orbit (if $\omega < \lambda_4$) or more complex chaotic if $\omega \gg \lambda_4$ and $I - I_{\text{homoclinic}}$ is not too small. This attractor manifests itself as a periodic solution in a simulation if the precision is not too high.
4. There exists a sequence of intervals $\mathbf{I}_n$ clustering at $I_{\text{homoclinic}}$ and an integer N_n assigned to each interval such that for all $I \in \mathbf{I}_n$, given any doubly infinite sequence of positive integers $\ldots n_{-1} n_0 n_1 n_2 \ldots$, with $n_i \geq N_n$, there exists a solution for which ξ executes n_i oscillations on the ith revolution of the center of mass η. This is explained by the fact that as $I \to I_{\text{homoclinic}}$, the movement of the spiral through the section S_0 causes the appearance of the horseshoe maps as subsystems of the maps S [Moser, 1973].

The number of relative oscillations of the pendula is determined by the integer label of the strip in the horseshoe map, and can be controlled by a proper choice of the integer sequence (cf. Moser [1973]).

There are many finer details of the picture that one can bring out [Ovsyannikov & Shil'nikov, 1987, and others], but we stop here, since the physical manifestation of most of these details is not observed numer-

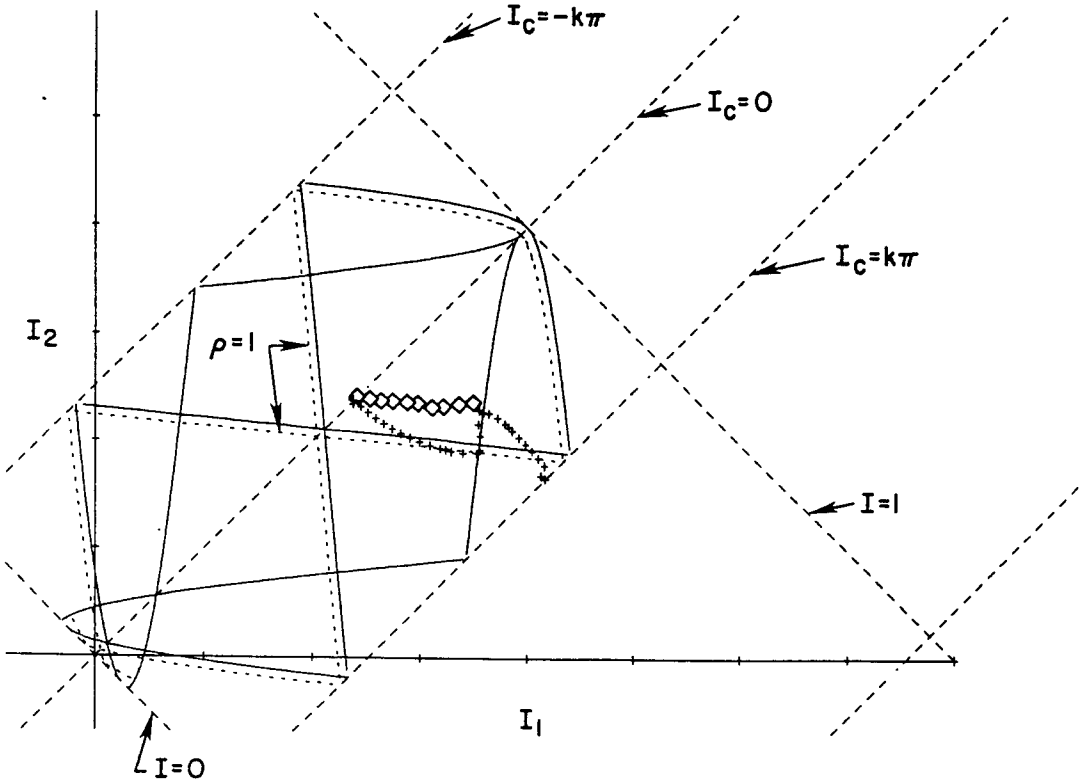

Fig. 14. Computed nearly homoclinic connections as a function of both torques I_1 and I_2 for $k=0.1$, $\gamma=0.5$. Near-homoclinic connections with two tumbles per period are marked with diamonds.

ically in this particular system due to the smallness of the basins of attraction. For instance, the invariant Cantor set of the horseshoe that gives us the sequences of integers has zero measure and thus zero probability of being observed as an asymptotic state. It must be pointed out, however, that the set's significance may rather lie in the fact that it may serve as a shared basin boundary of different sinks, i.e., as a "watershed" between different stable regimes.

The higher period Newhouse sinks have a small measure of the basins, and they do not show up numerically as well.

Remark. Shil'nikov heteroclinic bifurcation is of codimension two, since we have to satisfy two scalar equations, assuring that each of the one-dimensional unstable manifolds hits the appropriate three-dimensional stable manifold in $\mathbb{R}^4$. Only isolated curves in the three-dimensional parameter space (I_1, I_2, k) (or isolated points in the (I_1, I_2)-plane) satisfy the heteroclinic condition, thus creating an impression that the phenomena observed here should occur rarely. There are two factors that invalidate this impression to some extent. First, some of the connections occur along the symmetry line $I_c = k\pi$, so in the space of systems with such symmetry Shil'nikov heteroclinic bifurcations are of codimension one, and second, the neighborhoods of isolated points where the Shil'nikov heteroclinic behavior is manifesting itself is quite large numerically. For these values of k and γ, we see homoclinic orbits which spend time near a second, almost symmetric equilibrium point, for values of I_c down to $0.9k\pi$.

Remark. *Secondary homoclinic bifurcations.* We give a brief description of the secondary homoclinic connections, i.e., the connections in which the unstable manifold makes two or more passes in the region away from the neighborhood of the saddle-focus. Let C denote the center of the spiral, i.e., the point of intersection of W^u with the Poincaré section S_0. We let the parameter b decrease toward 0 and observe the resulting change of the image point $F_b(C)$. *If this point lies on the stable manifold $x_4 = 0$, then the solution $z(t)$ with $z(0) = C$ is doubly homoclinic.* Indeed, following this solution, i.e., the motion of the point C backward in time, we observe that it makes one global loop in a tubular neighborhood of W^u, crosses the Poincaré section S_1 going downward (i.e., with x_4 decreasing) and approaches the saddle-focus as $t \to -\infty$. Forward in time, $z(t)$ makes one loop following a tubular neighborhood of W^u and enters the plane $\{x_4 = 0\}$, and hence stays forever in the δ-neighborhood of the saddle-focus approaching it for $t \to -\infty$. We conclude that the corresponding solution makes two passes in the global region before re-entering

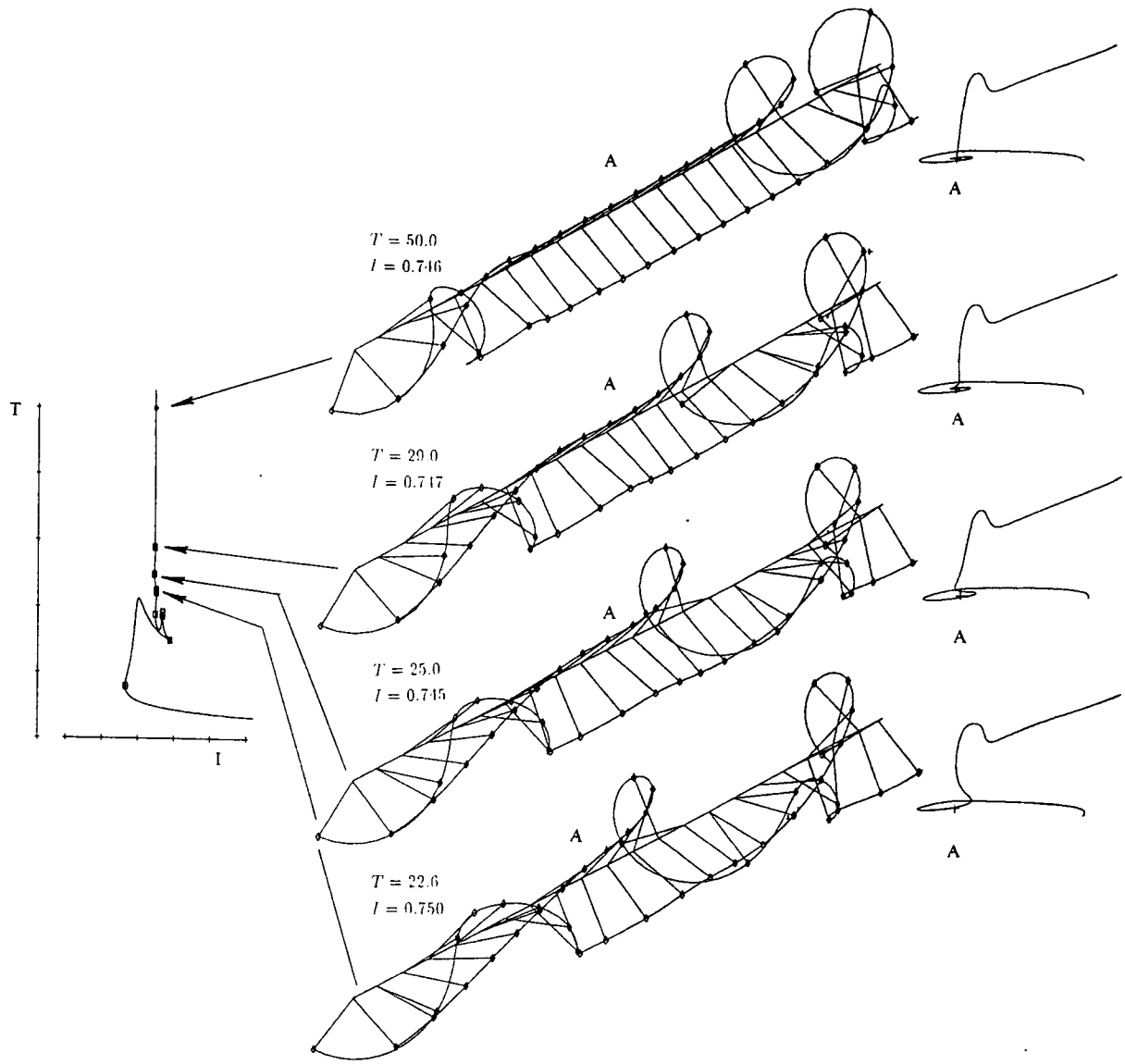

Fig. 15. Solutions at $k = 0.1$, $\gamma = 0.5$, $I_c = 0.7k\pi$, near the homoclinic orbit. The superimposed time traces of both pendula are shown for one complete orbit, together with a projection of the trajectory onto the eigenspace of the saddle-focus. The stable manifold is horizontal, the unstable one is vertical.

the neighborhood of the saddle-focus forever.

We give a brief heuristic description which shows that infinitely many such doubly homoclinic solutions arise for $b \downarrow 0$ in the case of $\rho < 1$. As $b \downarrow 0$, the point C is moving down, i.e., toward $x_4 = 0$; its image, therefore, travels along the spiral towards its center. In addition to that, the spiral itself moves down, with its center approaching $x_4 = 0$. In the case $\rho < 1$, when the spiral is "tight" on the outside, the distance between the point $F_b(C)$ and the center C of the spiral is much larger than the distance $O(b)$ from the center of the spiral to the stable manifold $\{x_4 = 0\}$. This shows that the point $F_b(C)$ runs *wide* circles around C (like a dog around its master) and consequently will cross $\{x_4 = 0\}$ infinitely many times before C does, thus implying the existence of infinitely many parameter values for which there are doubly homoclinic connections. The above argument can be made into a rigorous proof.

The existence of higher-order homoclinic connections can be shown in a similar way. We also point out that these multiply homoclinic orbits can be viewed in the context of symbolic dynamics as the "escape orbits", i.e., the solutions whose corresponding sequence terminates at both ends, in analogy with the escape in Sitnikov's problem in celestial mechanics, where a mass point can make any prescribed number

of oscillations and escape in the past time, future time, or both [Moser, 1973].

7. Caterpillar solutions and Shil'nikov's periodic solutions

Numerical evidence indicates a close similarity between the Shil'nikov solutions and the caterpillar solutions. In this section, we point out the difference and the similarity between the underlying geometro-analytic origins for the existence of these two types of solutions.

Caterpillar solutions have been discovered experimentally [Sullivan & Zimmerman, 1971] and numerically [Imry & Schulman, 1978]. Their nature was described in the introduction. What is important for us in the present discussion is the fact that the caterpillar solutions "make a turn" in $\mathbb{R}^4$ (which in fact looks like a 90-degree turn when projected into the (ϕ_1, ϕ_2)-plane), i.e., the pendula exchange motion, in the "shadow" of a bifurcated equilibrium solution. By contrast, the Shil'nikov solutions experience a similar exchange of motion, but it occurs near the saddle point on the homoclinic connection. That this causes one pendulum to stop and the other to "run" is clear from the eigenvectors at the saddle point. Locally W^u is approximated by the unstable eigenvector. For small k, $\alpha_0 = -\min(a, b) + O(k)$ and $\alpha_1 = -\max(a, b) + O(k)$. For $b > a$ and $a + b > 0$ (the case $a + b < 0$ is similar), the unstable manifold is approximately

$$W^u = (b - a, 0, \lambda_{00}(b - a), 0)^T + O(k) ,$$

and for $a > b$ and $a + b > 0$

$$W^u = (0, a - b, 0, \lambda_{00}(a - b))^T + O(k) .$$

The eigenvectors corresponding to the complex conjugate pair of eigenvalues are, for $b > a$ and $a + b > 0$,

$$v_{n1} = (0, a - b, 0, \lambda_{n1}(a - b))^T + O(k) ,$$

and for $a > b$ and $a + b > 0$,

$$v_{n1} = (b - a, 0, \lambda_{n1}(b - a), 0)^T + O(k) .$$

Therefore, near the Shil'nikov homoclinic connection, trajectories approach the equilibrium point with one pendulum nearly at rest, and leave with the other at rest. Which pendulum rests depends on the relative size of $\cos \phi_1$ and $\cos \phi_2$ and the sign of $\cos \phi_1 + \cos \phi_2$.

The following figures show the (ϕ_1, ϕ_2)-plane for various computed solutions. Figure 16 shows the synchronous solution, which is a diagonal motion, and the primary homoclinic solution, for $I_c = 0.1k\pi$ (see Fig. 10). The solutions on the period-doubled branch show the typical caterpillar-type motion, with the 90 degree turn far from the saddle point. The doubled homoclinic connection appears to avoid the eigenspace of the complex conjugate eigenvectors, approaching the saddle-focus along the eigenspace of the real, stable eigenvalue.

Figure 17 shows the same plots for solutions at $I_c = 0.55k\pi$. Here the homoclinic motion labeled A (see Fig. 11) makes one turn near the saddle, and the other near a second pair of equilibrium points. Homoclinic motions B and C exist at a larger value of I, at which the second pair of equilibrium points has disappeared in a saddle-node bifurcation. These have one turn which is like the caterpillar solution, and one which is not.

Finally Fig. 18 shows solutions at $I_c = 0.975k\pi$ (see Fig. 13). It is clear that the motions are almost heteroclinic, with both turns near equilibrium points.

The similarity between the caterpillar solutions and the Shil'nikov solutions is striking, but their nature is different. Stated loosely, the distinction between the

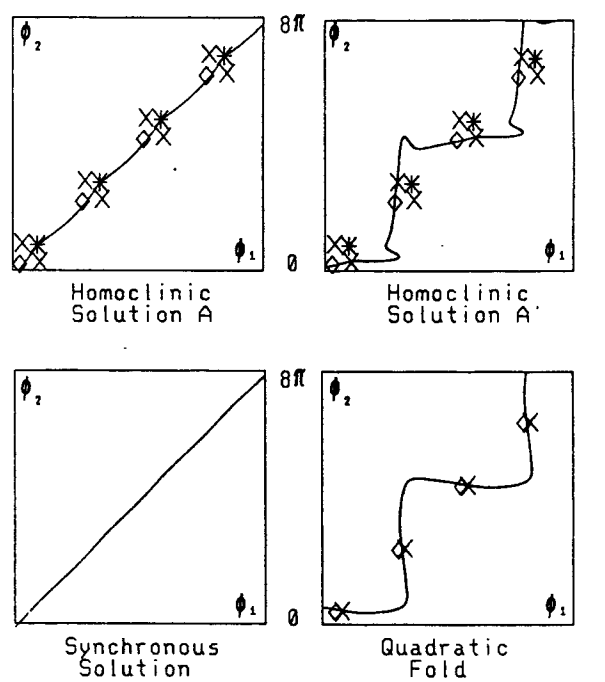

Fig. 16. Projections of the phase plane for various solutions from Fig. 10. Equilibrium points are marked. A diamond indicates a stable equilibrium, a cross one with two stable and two unstable eigenvalues, and a star an equilibrium with four unstable eigenvalues.

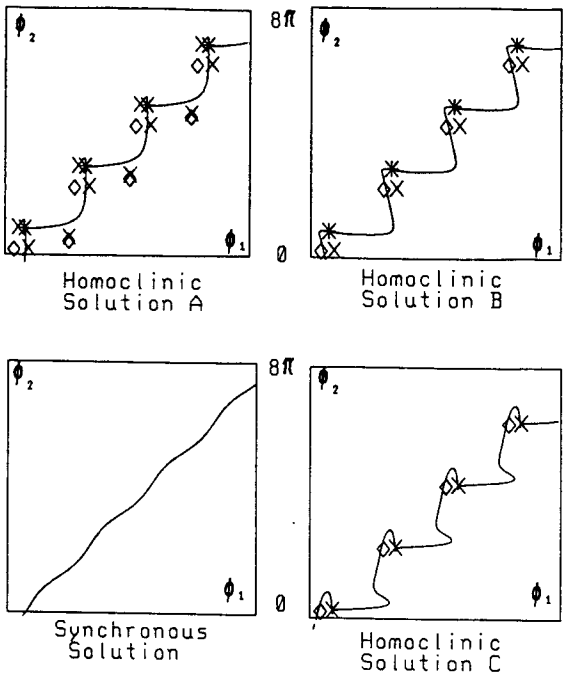

Fig. 17. Projections of the phase plane for various solutions from Fig. 11. Markings are the same as in Fig. 16.

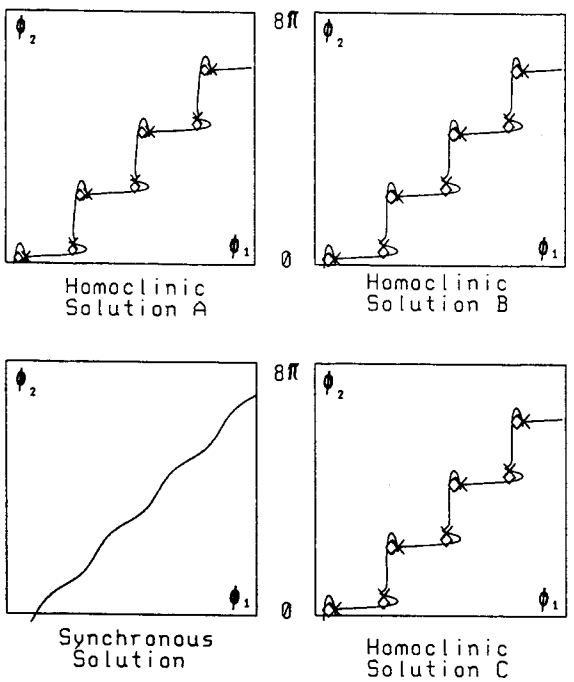

Fig. 18. Projections of the phase plane for various solutions from Fig. 13. Markings are the same as in Fig. 16.

"caterpillars" and the Shil'nikov-type solutions is that the former arise in the wake of a saddle-node bifurcation of equilibrium solutions, while the latter live in the neighborhood of a saddle-focus homoclinic loop.

Acknowledgement

The numerical investigation presented here was prompted by results of W. Liniger, which suggested the existence of period-doubling bifurcations from the branch of periodic solutions connected to the synchronous solution.

References

Amerio, L. [1949] "Determinazione delle condizioni di stabilita per gli integrali di una equazione interessante l'elettrotecnica", *Ann. Mat.* **4**(30), 75–90.

Andronov, A. A., Vitt, E. A. & Khaikin, S. E. [1949] *Theory of Oscillations* (Princeton Univ. Press).

Arnold, V. I. [1983] *Geometrical Methods in the Theory of Ordinary Differential Equations* (Springer).

Aronson, D. G., Doedel, E. J. & Othmer, H. G. [1991] "The dynamics of coupled current-biased Josephson junctions — Part II", *Int. J. Bifurcation and Chaos* **1**(1), 51–66.

Aubry, S. & LeDaeron, L. [1983] "The discrete Frenkel–Koutorova model and its extensions", *Physica* **8D**, 381–422.

Benedicks, M. & Carleson, L. [1988] "The dynamics of the Henon map", preprint.

Beyn, W.-J. [1987] "The effect of discretization on homoclinic orbits", in *Bifurcation: Analysis, Algorithms and Applications*, eds Kupper, T., Seydel, R. & Troger, H. (Birkhauser ISNM series, no. 79) pp. 1–8.

Conley, C. [1978] "Isolated invariant sets and the Morse index", CMBS 38 (AMS, Providence).

Doedel, E. J., Aronson, D. G. & Othmer, H. G. [1988] "The dynamics of coupled current-biased Josephson junctions: I", *IEEE Trans. Circuits and Systems* **35**(7), 810–817.

Doedel, E. J. & Friedman, M. J. [1989] "Numerical computation of heteroclinic orbits", *J. Comput. Appl. Math.* **26**, 155–170.

Doedel, E. J., Jepson, A. D. & Keller, H. B. [1984] "Numerical methods for Hopf bifurcation and continuation of periodic solution paths", in *Computing Methods in Applied Sciences and Engineering VI*, eds Glowinski, R. & Lions, J. L. (North-Holland).

Feynman, R. [1963] *The Feynman Lectures on Physics* (Addison-Wesley).

Glendinning, P. & Sparrow, C. [1984] "Local and global behavior near homoclinic orbits", *J. Stat. Phys.* **35**(5,6), 645–696.

Grüner, G. & Zettl, A. [1985] "CDW conduction: A novel collective transport phenomenon in solids", *Phys. Rep.* **119**(3), 119–232.

Holodiniok, M. & Kubiček, M. [1984] "DERPER — An algorithm for the continuation of periodic solutions in ordinary differential equations", *J. Comp. Phys.* **55**, 254–267.

Imry, Y. & Schulman, L. [1978] "Qualitative theory of the nonlinear behavior of coupled Josephson junctions", *J. Appl. Phys* **49**(2), 749–758.

Keller, H. B. [1977] "Numerical solution of bifurcation and nonlinear eigenvalue problems", in *Applications of Bifurcation Theory*, ed. Rabinowitz, P. H. (Academic Press, New York) pp. 359–384.

Keller, H. B. & Jepson, A. D. [1984] "Steady state and periodic solution paths: Their bifurcations and computations, in *Bifurcation: Analysis, Algorithms and Applications*, eds. Kupper, T., Mittelmann, H. D. & Weber, H. (Birkhauser ISNM series, no. 70) pp. 219–246.

Levi, M. [1988] "Caterpillar solutions in coupled pendula", *Erg. Th. Dyn. Sys.* **8**, 153–174.

Levi, M., Hoppensteadt, F. C. & Miranker, W. L. [1978] "Dynamics of the Josephson junction", *Quarterly of Appl. Maths.* (July 1978) 167–198.

Maginu, K. [1983] "Spatially homogeneous and inhomogeneous oscillations and chaotic motions in the Josephson junction line", *SIAM J. Appl. Math.* **43**(2), 225–243.

Marcus, P. M. & Imry, Y. [1980] "Steady oscillatory states of a finite Josephson junction", *Solid State Commun.* **33**, 345–349.

Mather, J. [1982] "Existence of quasi-periodic orbits for twist homomorphisms", *Topology* **21**, 457–467.

Moser, J. K. [1973] *Stable and Random Motions in Dynamical Systems*, Study 77 (Princeton University Press).

Ovsyannikov, I. M. & Shil'nikov, L. P. [1987] "On systems with a saddle-focus homoclinic curve", *Math. USSR Sbornik* **58**(2), 557–573.

Sullivan, D. B. & Zimmerman, J. E. [1971] "Mechanical analogs of time dependent Josephson phenomena", *Am. J. Phys.* **39**(12), 1504–1517.

Tricomi, F. [1931] "Sur une équation differentielle de l'electrotechnique", *C.R. Acad. Sci. Paris* **193**, 635–636.

Yakubovich, V. I. & Starzhinskii, V. M. [1975] *Linear Differential Equations with Periodic Coefficients.* (Wiley, NY).

Zimmerman, J. E. & Sullivan, D. B. [1977] "High-frequency limitations of the double-junction SQUID amplifier", *Appl. Phys. Lett.* **31**(5), 360–362.